PLOS ONE

RESEARCH ARTICLE

Biofluid modeling of the coupled eye-brain system and insights into simulated microgravity conditions

Fabrizia Salerni[1], Rodolfo Repetto[2], Alon Harris[3], Peter Pinsky[4], Christophe Prud'homme[5], Marcela Szopos[6], Giovanna Guidoboni[7]*

1 Department of Mathematical, Physical and Computer Sciences, University of Parma, Parma, Italy, **2** Department of Civil, Chemical and Environmental Engineering, University of Genoa, Genoa, Italy, **3** Eugene and Marilyn Glick Eye Institute and Department of Ophthalmology, Indiana University School of Medicine, Indianapolis, IN, United States of America, **4** Department of Mechanical Engineering, Stanford University, Stanford, CA, United States of America, **5** Institute of Advanced Mathematical Research UMR 7501, University of Strasbourg CNRS, Strasbourg, France, **6** Laboratoire MAP5 (UMR CNRS 8145), Université Paris Descartes, Sorbonne Paris Cité, France, **7** Department of Electrical Engineering and Computer Science, Department of Mathematics, University of Missouri, Columbia, MO, United States of America

* guidobonig@missouri.edu

Citation: Salerni F, Repetto R, Harris A, Pinsky P, Prud'homme C, Szopos M, et al. (2019) Biofluid modeling of the coupled eye-brain system and insights into simulated microgravity conditions. PLoS ONE 14(8): e0216012. https://doi.org/10.1371/journal.pone.0216012

Editor: Sakamuri V. Reddy, Charles P. Darby Children's Research Institute, Charleston, SC, UNITED STATES

Received: April 1, 2019

Accepted: July 8, 2019

Published: August 14, 2019

Data Availability Statement: The data utilized in the model simulation are fully included in the body of the paper.

Funding: This work has been partially supported by the award NSF DMS-1853222/1853303, the Chair Gutenberg funds of the Cercle Gutenberg (France) and the Labex IRMIA and the IdEx Unistra (University of Strasbourg, France).

Competing interests: The authors have declared that no competing interests exist.

Abstract

This work aims at investigating the interactions between the flow of fluids in the eyes and the brain and their potential implications in structural and functional changes in the eyes of astronauts, a condition also known as spaceflight associated neuro-ocular syndrome (SANS). To this end, we propose a reduced (0-dimensional) mathematical model of fluid flow in the eyes and brain, which is embedded into a simplified whole-body circulation model. In particular, the model accounts for: *(i)* the flows of blood and aqueous humor in the eyes; *(ii)* the flows of blood, cerebrospinal fluid and interstitial fluid in the brain; and *(iii)* their interactions. The model is used to simulate variations in intraocular pressure, intracranial pressure and blood flow due to microgravity conditions, which are thought to be critical factors in SANS. Specifically, the model predicts that both intracranial and intraocular pressures increase in microgravity, even though their respective trends may be different. In such conditions, ocular blood flow is predicted to decrease in the choroid and ciliary body circulations, whereas retinal circulation is found to be less susceptible to microgravity-induced alterations, owing to a purely mechanical component in perfusion control associated with the venous segments. These findings indicate that the particular anatomical architecture of venous drainage in the retina may be one of the reasons why most of the SANS alterations are not observed in the retina but, rather, in other vascular beds, particularly the choroid. Thus, clinical assessment of ocular venous function may be considered as a determinant SANS factor, for which astronauts could be screened on earth and in-flight.

Introduction

Microgravity conditions have been observed to induce structural and functional changes in the eyes of many astronauts that pose serious challenges for both astronauts and their missions in space [1–3]. This syndrome, also known as spaceflight associated neuro-ocular syndrome (SANS), is characterized by a large number of apparently unrelated and often not concurrent symptoms. These include choroidal folds, cotton wool spots, optic nerve distension and/or kinking, optic disc protrusion, posterior globe flattening, refractive deficits and elevated intracranial pressure [1, 4]. Added to the complexity of the range of symptoms are the problems of susceptibility and genetic predisposition to develop visual problems.

The current understanding of how weightlessness environment affects the human body and may lead to SANS development is still quite rudimentary. Various studies of the symptoms experienced by astronauts during long-term missions (four to six months) have been performed [2], but their validity is hampered by the small size of the subjects cohort. To overcome this difficulty, ground-based microgravity laboratory models have been proposed, the most significant of which is the long head down tilt (LHDT) experimental procedure that is used to simulate the effects of microgravity on the cardiovascular system. LHDT experiments have shown that the fluid shift caused by the tilt produces a transient increase in central venous pressure, later followed by an increase in left ventricular size without changes in cardiac output, arterial pressure, or contractile state [5]. Moreover, experiments performed by [6] confirmed that microvascular pressures measured in the lower lip increase, as well as subcutaneous and intramuscular interstitial fluid pressures in the neck. Interestingly, interstitial fluid colloid osmotic pressures remain unchanged, whereas plasma colloid osmotic pressures drop significantly after 4 hours of LHDT, thereby suggesting a transition from fluid filtration to absorption in capillary beds between the heart and feet during LHDT. The above-mentioned studies suggest that two main mechanisms may be involved in SANS pathophysiology, namely: *(i)* changes in the vascular system and fluid distribution (fluid shifts); and *(ii)* changes in the brain/central nervous system and intracranial pressure (ICP). However, experimental results are not always consistent among studies. For example, optic disc edema, which is one of the ocular findings associated with SANS, was not observed in the LHDT study conducted by Taibbi et al [7], whereas it was observed in the study conducted by Laurie et al [8]. This discrepancy in the results might be due to different protocols adopted for the study, such as the extent to which head tilt was enforced, and the fact that many factors may influence ocular structural and functional changes, including blood pressure, intraocular pressure (IOP) and cerebrospinal fluid pressure (CSFp), which may vary among individuals and are difficult to isolate in an experimental setting.

A complementary approach to experimental studies is the use of mathematical modeling as a tool to investigate theoretically the role of various factors potentially contributing to SANS and help elucidate the mechanisms of their interactions and their implications in structural and functional changes in the eye. To the best of our knowledge, the mathematical modeling of hemo-fluid dynamic contributions to SANS is still at its early stages. A lumped-parameter model to simulate volume/pressure alterations in the eye in zero gravity conditions was presented in [9]. The model includes the effects of blood and aqueous humor dynamics, ICP, and IOP-dependent ocular compliance. A lumped-parameter model of fluid transport in the central nervous system aimed at simulating the influence of microgravity on ICP was presented in [10]. The model could be coupled, in the authors' intention, to lumped parameter and finite element models of the eye. The present work advances the modeling methods in the context of SANS by providing a more detailed description of fluid circulations in the eyes and their connections to the brain, as sketched in [11–14]. In particular, the model accounts for the blood

flow within three major ocular vascular beds, namely retina, choroid and ciliary body. The model describes the intimate connection between ocular and cerebral hemodynamics, as brain and eyes share vessels for blood supply and drainage. In addition, the cerebrospinal fluid (CSF) flowing within the subarachnoid space influences the tissue pressure in the optic nerve head and, as a consequence, the biomechanics and hemodynamics of the lamina cribrosa and the vessels running through it. The model is used to investigate the complex relationship between blood pressure, IOP, ICP, CSFp and the flow of fluids within eyes and brain, which are thought to be important factors contributing to SANS.

Interestingly, the modeling ingredients embedded in the proposed model make it a very flexible tool to study interactions between the eyes and the rest of the body, particularly the brain, in various conditions beyond the microgravity environment. Thus, besides the application to SANS discussed in the present work, we believe that the proposed model could serve as a basic framework to study pathological states, most importantly glaucoma [15–17], where the interaction between ocular and cerebral hemo-fluid-dynamics is thought to play an important role. Specifically, it is well-documented that the levels of blood pressure, IOP and CSFp, along with other vascular and biomechanical risk factors, strongly affect etiology, progression and incidence of glaucoma [18–22]. As medicine is clearly heading in the direction of tailored diagnosis and treatment, the clinical ability to ascertain the relative weight of each risk factor in any given patient is of paramount significance. Although the use of imaging technology in medicine has advanced in giant steps in recent years, there is no clinical standard for quantifying all relevant clinical outcomes in any given subject. In this perspective, mathematical modeling can provide a virtual lab where the clinical significance of each risk factor can be quantified and novel individualized therapeutic approaches can be designed [23].

The paper is organized as follows. We begin by providing a description of the mathematical model, which is articulated in four main parts, first outlining its general characteristics, then describing in more detail the model of the brain, of the eyes and of their coupling. We then discuss how microgravity conditions are modeled and how the overall system is solved numerically. A description of the rationale adopted for model calibration is followed by an outline of the model validation against experimental observations. The paper ends with the results of model simulations and their critical discussion.

Materials and methods

Lumped parameter mathematical model

General description of the model. We propose a lumped parameter model of the brain and eyes, connected with a highly simplified model of the body, the electrical analogue of which is shown in Fig 1. The aim of the model, which describes pressure and flow distributions in the brain and eyes, is to predict fluid redistribution in the upper body vasculature and variations of the IOP and ICP following exposure to a microgravity environment.

The physiological system is subdivided into a number of linked, interacting compartments, each of which contains a single physical constituent, such as blood, cerebrospinal fluid, interstitial fluid and aqueous humor. In particular, we consider the interactions among the following components (see Fig 1):

in the brain:

- blood (3 compartments: intracranial arteries (I), capillaries (C), intracranial venous sinuses (S));
- cerebrospinal fluid (1 compartment: ventricular CSF (F));

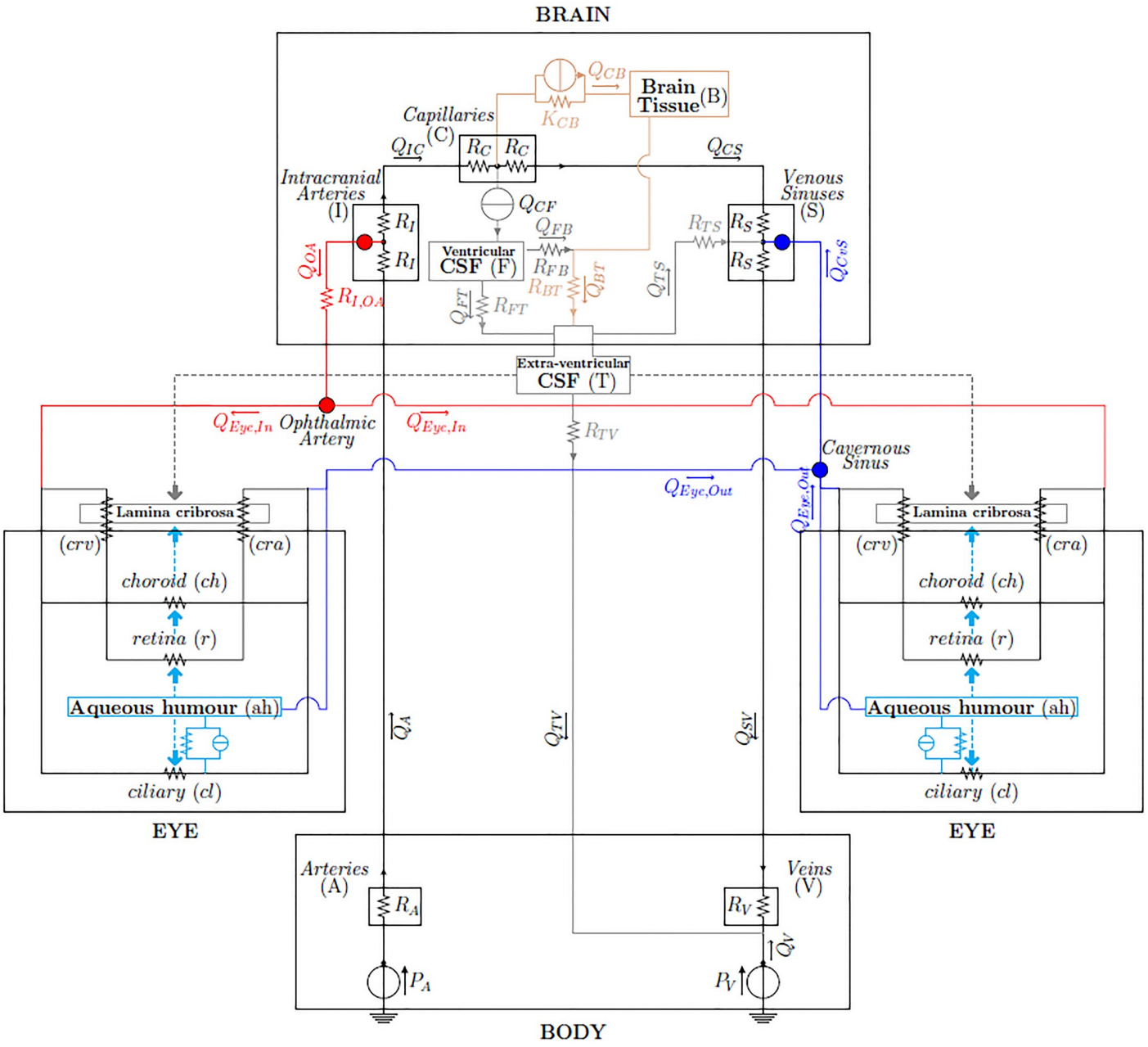

Fig 1. Network model of fluid flows in the brain and eyes [12–14]. The nodes correspond to the connection between the brain and eye models. The connection *Intracranial Arteries-Ophthalmic Artery* represents arterial supply; the connection *Venous Sinuses-Cavernous Sinus* represents the venous drainage; the grey and cyan arrows represent the pressures acting on both sides of the lamina cribrosa.

https://doi.org/10.1371/journal.pone.0216012.g001

- cerebral tissue and interstitial fluid (1 compartment: brain (B));

  in each of the two eyes:

- blood (5 compartments: retina (*r*), choroid (*ch*), central retinal artery (*cra*), central retinal vein (*crv*), ciliary body circulation (*cl*));
- aqueous humor (*ah*) (1 compartment: anterior and posterior chamber);

and in the eye-brain coupling:

- cerebrospinal fluid (1 compartment: extra-ventricular (T) bridging intracranial and extracranial regions, also including the subarachnoid space in the optic nerve posterior to the lamina cribrosa).

The lumped parameter circuit for the brain adopted in the present work was described and validated by Lakin and Stevens in [24] for microgravity simulations. The eye block combines a model for the retinal circulation and a model for the dynamics of aqueous humor that have been proposed by some of the authors of this paper in [25] and [26], respectively, and extends them to account also for the choroidal and ciliary body vascular beds [27]. In this work, we focus on the mean behavior of the system and we neglect time variations on both the short time scale of the heart beat and on the long time scale of remodelling processes. We also neglect autoregulation mechanisms of small vessels, since we wish to keep the model relatively simple in order to understand its basic behaviour. Moreover, little information exists about autoregulation mechanisms in orbit, except that they might be altered due to high CO_2 concentrations [1, 2].

The brain and eye models are coupled to each other and are linked to the rest of the body via a highly simplified model consisting of two compartments: central arteries (A) and central veins (V). This description corresponds to a model for the human physiology of the upper part of the body. Throughout the paper, lower case letters will denote compartments in the eyes and upper case letters will denote compartments in the brain and body.

Two main types of flows are included in the model, namely *filtration* and *pressure-driven flows*. Fluid filtration is accounted for in two instances: *(i)* filtration of interstitial fluid from the capillaries to the interstitial space, with the associated flow denoted by Q_{CB}, and *(ii)* filtration of aqueous humor from the ciliary body capillaries into the posterior/anterior chambers, with the associated flow denoted by J_{uf}. In general terms, the flux Q_{ij} due to filtration from the compartment i to the compartment j is modeled by the Starling-Landis equation [28]:

$$Q_{ij} = K_{ij}[(P_i - P_j) - \sigma_{ij}(\pi_i - \pi_j)], \tag{1}$$

where P_i and π_i are the hydraulic and osmotic pressures in the compartment i, whereas K_{ij} and σ_{ij} are the filtration and reflection coefficients from the compartment i to the compartment j. The electric analogue of the Starling-Landis Eq (1) is an element with a resistor and a current generator arranged in parallel, as depicted in Fig 1. All other flows in the model are simply driven by the hydraulic pressure difference between compartments. In this case, the pressure-driven flux Q_{ij} between the generic compartments i and j is governed by the hydraulic analogue of Ohm's law

$$Q_{ij} = \frac{P_i - P_j}{R_{ij}} \tag{2}$$

where R_{ij} denotes the hydraulic resistance. Each compartment i in the model is assumed to have a total resistance to flow of $2R_i$; then the resistance R_{ij} in Eq (2) is taken to be $R_{ij} = R_i + R_j$, i.e. the sum of half of the resistance of compartments i and j. In the following, owing to the complexity of the eye model, we will use different notations to identify the various components of the eye circuits.

By formulating the above equations for all compartments and by writing the Kirchhoff law of currents at all circuit nodes, we obtain a set of nonlinear algebraic equations in the unknowns P_i, as reported in Tables 1 and 2. The nonlinearity is a consequence of the fact that,

Table 1. Summary of the model equations obtained by writing the Kirchhoff current law at the circuit nodes.

Kirchoff Current Laws	
Brain	
Compartment I	$Q_A = Q_{OA} + Q_{IC}$
Compartment C	$Q_{IC} = Q_{CB} + Q_{CS} + Q_{CF}$
Compartment S	$Q_{CS} + Q_{TS} + Q_{CvS} = Q_{SV}$
Compartment B	$Q_{FB} + Q_{CB} = Q_{BT}$
Compartment F	$Q_{CF} = Q_{FT} + Q_{FB}$
Compartment T	$Q_{FT} + Q_{BT} = Q_{TV} + Q_{TS}$
	$Q_V = Q_{TV} + Q_{SV}$
Eye	
Node 1	$Q_{Eye,In} = Q_{cl} + Q_{ch} + Q_r$
Node 2	$Q_{cl} = Q_{cl,v} + J_{uf}$
Node 3	$Q_{cl,v} + Q_{ch} + Q_r + J_{tm} = Q_{Eye,Out}$
Node 4	$J_{uf} + J_{secr} = J_{ah}$
Node 5	$J_{ah} = J_{uv} + J_{tm}$
Body-Brain-Eye Coupling	
Ophthalmic Arteries	$Q_{OA} = 2Q_{Eye,In}$
Cavernous Sinus	$Q_{CvS} = 2Q_{Eye,Out}$

https://doi.org/10.1371/journal.pone.0216012.t001

in some compartments, resistances are assumed to depend on pressures. This is discussed in the following sections, where the brain and eye models are described in more detail.

The brain model

The human brain is a fully enclosed organ and its tissue is a medium saturated by three different fluids interacting with each other: *(i)* blood, *(ii)* cerebrospinal fluid and *(iii)* interstitial fluid. The cerebrospinal fluid is produced mainly by the choroid plexus. It flows through the ventricular system to the subarachnoid space, where it is absorbed into the blood stream via the sagittal sinus. The interstitial or extracellular fluid fills the interstices of the brain tissue, bathing the neurons. In healthy subjects, only a relatively small amount of fluid is able to leak from blood into the interstitial fluid, owing to the low permeability of the blood-brain barrier [29].

In this work, we describe the brain via an electrical analogue representation of the model proposed by Lakin and Stevens in [24], as schematically shown in the "BRAIN" box of Fig 1. The model consists of three fluid networks: *(i)* the blood vasculature (Fig 1, black portion), *(ii)* the cerebrospinal fluid network (Fig 1, grey portion) and *(iii)* the interstitial fluid network (Fig 1, tan portion). The brain model is connected to the upper part of the body through the systemic central arteries (A) and veins (V) compartments characterized by the resistances R_A and R_V, respectively. CSF production is externally imposed and kept constant at the production rate Q_{CF}. Unlike the choice adopted in [24] to impose a constant flux Q_{IC} between the intracranial arteries and the capillaries accounting for the autoregulation of cerebral blood flow, here we allow cerebral blood flow to change by inserting the hydraulic resistances R_I and R_C between the compartments I and C. An extra-ventricular compartment (T) filled with cerebrospinal fluid bridges the intracranial and extracranial regions and includes the subarachnoid space in the optic nerve, posterior to the lamina cribrosa.

We remark that, among the numerous models that have been proposed to simulate cerebral fluid-dynamics (see e.g [24, 30–33]), in this work we have adopted the one proposed by

Table 2. Summary of the model balance and constitutive relations.

Constitutive Relations
Brain
Cerebral Blood Flow
$Q_{IC} = (P_I - P_C)/(R_I + R_C)$
$Q_{CS} = (P_C - P_S)/(R_C + R_S)$
Cerebrospinal and Interstitial Fluid Flow
$Q_{CB} = K_{CB}[(P_C - P_B) - \sigma_{CB}\,\Delta\pi_{CB}]$
$Q_{BT} = (P_B - P_T)/R_{BT}$
$Q_{FT} = (P_F - P_T)/R_{FT}$
$Q_{TS} = (P_T - P_S)/R_{TS}$
$Q_{FB} = (P_F - P_B)/R_{FB}$
Eye
Blood Flow
$Q_{cl} = (P_{Eye,In} - P_{cl,c})/(R_{cl,in} + R_{cl,a1} + R_{cl,a2} + R_{cl,c1})$
$Q_{cl,v} = (P_{cl,c} - P_{Eye,Out})/(R_{cl,c2} + R_{cl,v1} + R_{cl,v2} + R_{cl,out})$
$Q_{ch} = (P_{Eye,In} - P_{Eye,Out})/(R_{ch,in} + R_{ch} + R_{ch,out})$
$Q_r = (P_{Eye,In} - P_{Eye,Out})/(R_{cra,in} + R_{cra} + R_r + R_{crv} + R_{crv,out})$
$R_{ch} = R_{ch,a1} + R_{ch,a2} + R_{ch,c1} + R_{ch,c2} + R_{ch,v1} + R_{ch,v2}$
$R_{cra} = R_{cra,1} + R_{cra,2} + R_{cra,3} + R_{cra,4}$
$R_r = R_{r,a1} + R_{r,a2} + R_{r,c1} + R_{r,c2} + R_{r,v1} + R_{r,v2}$
$R_{crv} = R_{crv,1} + R_{crv,2} + R_{crv,3} + R_{crv,4}$
$R_{i,v1} = R_{i,v2} = \begin{cases} \alpha_i(1 + (P_{i,v} - \mathrm{IOP})/(k_{p,i}k_{L,i}))^{-4} & \text{if } P_{i,v} > \mathrm{IOP} \\ \alpha_i(1 - (P_{i,v} - \mathrm{IOP})/k_{p,i})^{4/3} & \text{if } P_{i,v} \le \mathrm{IOP} \end{cases}$ for $i = cl, ch, r$
$\alpha_i = 8\pi\mu_v\mathcal{L}_v/\mathcal{A}_{i,v}^2$ for $i = cl, ch, r$
$k_{p,i} = E_v h_v^3 \pi^{3/2}/(12(1 - v_v^2)\mathcal{A}_{i,v}^{3/2})$ for $i = cl, ch, r$
$k_{L,i} = 12\mathcal{A}_{i,v}/(\pi h_v^2)$ for $i = cl, ch, r$
$R_{cra,n} = \alpha_{cra,n}(1 + \Delta P_{cra,n}/(k_{p,cra,n}\,k_{L,cra,n}))^{-4}$ for $n = 1, 2, 3, 4$
$\Delta P_{cra,1} = (P_{cra,in} + P_{cra,1})/2 - P_T$
$\Delta P_{cra,2} = (P_{cra,1} + P_{cra,2})/2 - P_T$
$\Delta P_{cra,3} = (P_{cra,2} + P_{cra,3})/2 - P_{LC}$
$\Delta P_{cra,4} = (P_{cra,4} + P_{cra,4})/2 - \mathrm{IOP}$
$\alpha_{cra,n} = 8\pi\mu_{cra}\mathcal{L}_{cra,n}/\mathcal{A}_{cra}^2$ for $n = 1, 2, 3, 4$, with $\mathcal{A}_{cra} = \frac{\pi D_{cra}^2}{4}$
$k_{p,cra,n} = E_{cra} h_{cra}^3 \pi^{3/2}/(12(1 - v_{cra}^2)\mathcal{A}_{cra,n}^{3/2})$ for $n = 1, 2, 3, 4$
$k_{L,cra,n} = 12\mathcal{A}_{cra,n}/(\pi h_{cra}^2)$ for $n = 1, 2, 3, 4$
$R_{crv,n} = \begin{cases} \alpha_{crv,n}(1 + \Delta P_{crv,n}/(k_{p,crv,n}k_{L,crv,n}))^{-4} & \text{if } \Delta P_{crv,n} > 0 \\ \alpha_{crv,n}(1 - \Delta P_{crv,n}/k_{p,crv,n})^{4/3} & \text{if } \Delta P_{crv,n} \le 0 \end{cases}$ for $n = 1, 2, 3, 4$
$\Delta P_{crv,1} = (P_{crv,1} + P_{crv,2})/2 - \mathrm{IOP}$
$\Delta P_{crv,2} = (P_{crv,2} + P_{crv,3})/2 - P_{LC}$
$\Delta P_{crv,3} = (P_{crv,3} + P_{crv,4})/2 - P_T$
$\Delta P_{crv,4} = (P_{crv,4} + P_{crv,out})/2 - P_T$
$\alpha_{crv,n} = 8\pi\mu_{crv}\mathcal{L}_{crv,n}/\mathcal{A}_{crv}^2$ for $n = 1, 2, 3, 4$, with $\mathcal{A}_{crv} = \frac{\pi D_{crv}^2}{4}$
$k_{p,crv,n} = E_{crv} h_{crv}^3 \pi^{3/2}/(12(1 - v_{crv}^2)\mathcal{A}_{crv,n}^{3/2})$ for $n = 1, 2, 3, 4$
$k_{L,crv,n} = 12\mathcal{A}_{crv,n}/(\pi h_{crv}^2)$ for $n = 1, 2, 3, 4$
Aqueous Humor Flow
$J_{uf} = L_{in}[(P_{cl,c} - \mathrm{IOP}) - \sigma_p\,\Delta\pi_p]$

(*Continued*)

Table 2. (Continued)

Constitutive Relations
$J_{uv} = \mathrm{IOP}/R_{uv}$
$R_{uv} = (k_2 + \mathrm{IOP})/k_1$
$J_{tm} = (\mathrm{IOP} - P_{evp})/R_{tm}$
$R_{tm} = R_0(1 + \kappa(\mathrm{IOP} - P_{evp}))$
Body-Brain-Eye Coupling
$Q_A = (P_A - P_I)/(R_A + R_I)$
$Q_{SV} = (P_S - P_V)/(R_S + R_V)$
$Q_{TV} = (P_T - P_V)/R_{TV}$
$Q_{OA} = (P_I - P_{Eye,In})/R_{I,OA}$
$P_{Eye,Out} = P_S$

https://doi.org/10.1371/journal.pone.0216012.t002

Lakin and Stevens in [24] because of its purpose to study the response of intracranial pressure in microgravity environments. Indeed, other choices could be made, in the perspective that specific blocks of the coupled model could be improved as research advances in the corresponding fields. For example, the model adopted here does not include the collapsibility of the internal jugular veins and the presence of the lymphatic and glymphatic systems that may contribute to fluid motion in the brain. To date, many issues regarding the anatomy and physiology of the venous and lymphatic systems, in the brain as well as in other parts of the body, are not completely understood. For example, the routes of venous drainage from the brain are quite complex and may vary with posture and external conditions [34–37]) and the mechanisms regulating the flow of lymph through the various parts of the brain are still under investigation [38, 39]. These aspects will be included in future developments of the work.

The eye model

The full model of the eye is schematically shown in the two "EYE" boxes of Fig 1 and is depicted in detail in Fig 2. It comprises two interconnected circuits hosting the flow of blood and aqueous humor, respectively. The vascular circuit (Fig 2, black portion) consists of three vascular beds, corresponding to the retinal, choroid and ciliary body circulations, arranged in parallel to each other. In the aqueous humor circuit (Fig 2, cyan portion) fluid is produced in the ciliary body via ultrafiltration and active secretion, and then drained via the trabecular and uveoscleral pathways. Inclusion of this circuit is important since the balance between aqueous production and drainage governs the levels of IOP. The light blue-shaded area in the figure represents the interior of the eye globe, where the pressure equals IOP. This means that all vessels in the circuits exposed to such an area are subjected to an external pressure equal to IOP. Finally, the grey-shaded area represents the lamina cribrosa, which is loaded by IOP on the one side and by the pressure within the optic nerve tissue on the other side, which is mainly due to the CSFp in the subarachnoid space [40]. The central retinal artery and vein running through the lamina are subjected to external mechanical actions that are produced by the deformation of the lamina [41, 42].

Further details of all eye circuits and the eye-brain coupling are provided in the following subsection.

The ocular vascular circuit. The main arterial supply to the eye is the ophthalmic artery, which branches from the carotid artery. The major branches of the ophthalmic artery are the

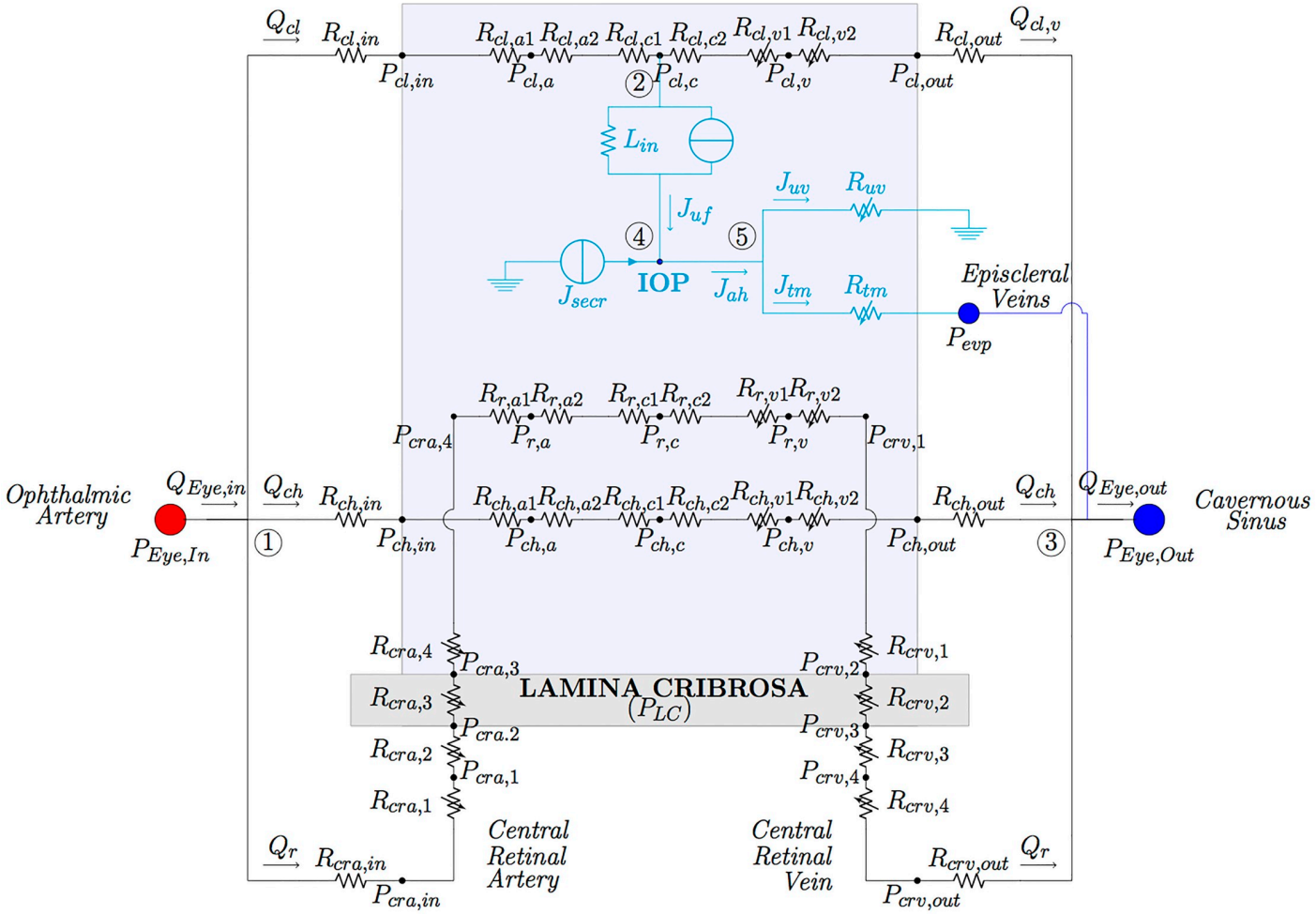

Fig 2. Network model for the eye vasculature (black portion) and aqueous humor production and drainage (cyan portion). The vasculature comprises circulation of blood in retinal, ciliary and choroidal vascular bed. Variable resistances are marked with arrows.

https://doi.org/10.1371/journal.pone.0216012.g002

long ciliary arteries, that nourish the ciliary body, the central retinal artery (*cra*) that nourishes the inner part of retina and the posterior ciliary arteries that nourish the choroid. Ciliary body and choroidal circulations drain into the superior ophthalmic vein, which exits the orbit through the superior orbital fissure and drains into the cavernous sinus. Retinal blood drainage occurs via the central retinal vein (*crv*) and eventually converges into the cavernous sinus. The *cra* and *crv* run through the optic nerve canal, piercing the lamina cribrosa approximately in its center.

Each vascular bed of the circuit is composed of three lumped compartments connected in series and representing arterioles (*a*), capillaries (*c*) and venules (*v*), as detailed in Fig 2. In the figure and the following text, the pressure in each node of the vascular circuit is denoted $P_{i,n}$, where $i = r, cl, ch, cra, crv$ indicates the different vascular segments (*r* for retina, *cl* for ciliary body, *ch* for choroid and *cra* and *crv* for the central retinal artery and vein, respectively) and *n* allows us to distinguish between different nodes within the same segment ($n = 1, 2, 3$ in the *cra* and *crv*, $n = a, c, v$ in the retinal, ciliary body and choroidal circulations, and $n = in, out$ in the vascular structures located before the arterioles and after the venules of the vascular segment *i*). A similar notation holds for all resistances; for instance, $R_{r,v2}$ denotes the resistance in the retinal circuit downstream of the node representative of retinal venule (with pressure $P_{r,v}$).

The vascular circuits include both constant and variable resistances. Constant resistances are calibrated at the reference state and their value is kept constant in all numerical simulations. In particular, constant resistances are adopted for arterioles and capillaries, since active changes in vascular diameters due to blood flow regulation are not accounted for in the present model. To characterize constant resistances, we used Poiseuille law to relate flux and pressure drop along each single vessel. This leads to the following expression for a generic resistance of each component of the circuit

$$R = \frac{k_r \rho \mathcal{L}}{\mathcal{A}^2}, \tag{3}$$

where $\mathcal{A}$ is the representative cross-sectional area of the compartment, $\mathcal{L}$ the representative compartment length, ρ is blood density, μ is blood dynamic viscosity and $k_r = 8\pi\mu/\rho$. In the case of a single vessel, $\mathcal{A}$ and $\mathcal{L}$ correspond to the vessel cross-sectional area and length respectively. Also note that the circuit has been constructed in such a way that the resistance of each compartment within the eye (arterioles, capillaries and venules) is split into two resistances with the same characteristics (see Fig 2), resulting in a node representing the mean pressure of the compartment.

Variable resistances are indicated by an arrow in Fig 2. They account for passive changes in vascular diameter and, possibly, shape of the cross-sectional area, due to the action of the transmural pressure difference ΔP_t (i.e. the pressure difference across the vessel wall) and the deformability of the vessel wall. Variable resistances are modeled by combining a *tube law*, describing the mechanical response of the vessel wall to changes in the transmural pressure difference, and *Poiseuille law*, describing the fluid flow through the resistor. Following [25] and [43], we model deformable tubes as Starling resistors, which reflect the physiological high collapsibility of the venous segments when the transmural pressure becomes negative. For a generic resistance R we then write

$$R = \begin{cases} \dfrac{8\pi\mu\mathcal{L}}{\mathcal{A}^2}\left(1 + \dfrac{\Delta p_t}{k_p\, k_L}\right)^{-4} & \text{if } \Delta p_t > 0, \\ \dfrac{8\pi\mu\mathcal{L}}{\mathcal{A}^2}\left(1 - \dfrac{\Delta p_t}{k_p}\right)^{4/3} & \text{if } \Delta p_t \leq 0, \end{cases} \tag{4}$$

where,

$$k_L = 12\frac{\mathcal{A}}{\pi h^2}, \qquad k_p = \frac{E h^3 \pi^{3/2}}{12(1-\nu^2)\mathcal{A}^{3/2}}, \tag{5}$$

where h, E and ν are thickness, Young's modulus and Poisson ratio of the vessel wall, respectively. The value of ΔP_t differs depending on the particular vascular segment under consideration, as specified in Table 2. In particular, in all circulation segments inside the eye (light blue shaded area in Fig 2) the pressure external to the vessel coincides with the IOP. On the other hand the translaminar segments of the central retinal artery and vein are subjected to an external radial compressive stress P_{LC} that originates within the lamina cribrosa as a consequence of the action of IOP, CSFp and scleral tension acting on it, as schematized in Fig 3 (left). In order to evaluate this compressive stress, we use the nonlinear elastic model proposed by some of the authors in [41], with the parameter choices reported in [25]. This three-dimensional numerical model is employed to compute P_{LC} for various values of IOP and CSFp forcing the lamina deformation. The results are reported with dots in Fig 3 (right)

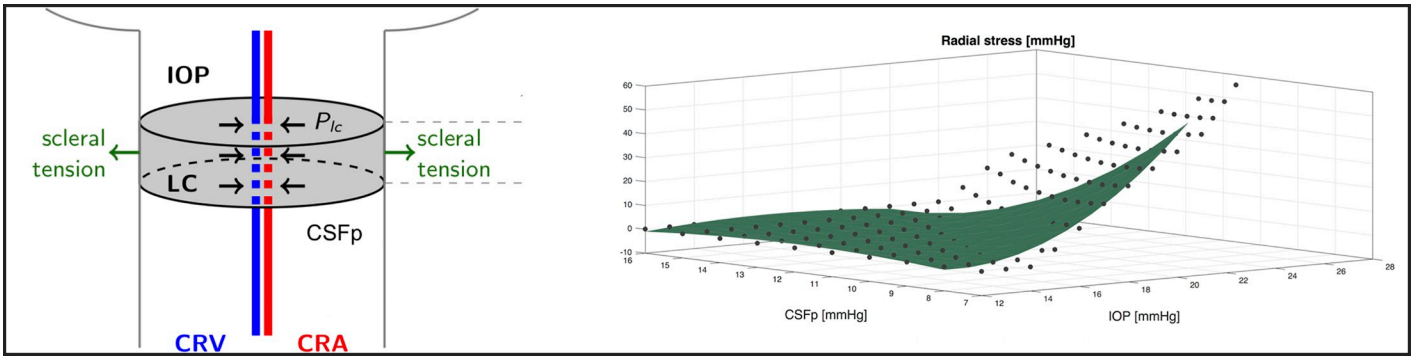

Fig 3. *Left*: Schematic representation of the radial compressive stress P_{LC} originating within the lamina cribrosa as a consequence of the action of IOP, CSFp and scleral tension acting on it. P_{LC} acts as external pressure on the translaminar segments of the central retinal artery and vein. *Right*: Magnitude of the radial compressive stress P_{LC} computed using the nonlinear elastic model described in [41] for various IOP and CSFp levels (black dots) and interpolated using using a second order polynomial function (green surface).

https://doi.org/10.1371/journal.pone.0216012.g003

and have been fitted using a second order polynomial function, shown in the figure by the green surface. Such a surface is then employed to determine the external pressure acting on the translaminar vascular segments.

We remark that, in the current version of the model, variable resistances are adopted only to simulate passive diameter changes in the ocular venous segments. In future extensions of the model, variable resistances could also be utilized to simulate diameter changes in the arterioles, where passive and active mechanisms could be included by introducing appropriate functional expressions relating changes in the representative cross-sectional area $\mathcal{A}$ to changes in biophysical factors, such as transmural pressure difference, shear stress, oxygen levels and pH (see e.g. [44–47]). Active changes in arteriolar diameter are the result of regulatory mechanisms whose presence and functionality on earth and in microgravity conditions are yet to be fully assessed. This is particularly true for the choroid, where the presence of regulatory mechanisms has been discovered only recently and remains, to date, vastly understudied [1, 48–50]. Interestingly, there have been reports that the choroid engorges during spaceflight [51], although, to date, choroidal flow has not been actually measured during spaceflight. Thus, it would be very interesting to include a more detailed description of choroidal hemodynamics in future developments of the model.

The aqueous humor circuit. The aqueous circuit used in this model was proposed by some of the authors in [26] and its electrical analogue is depicted in cyan in Fig 2. The value of IOP results from the balance between aqueous humor production and drainage.

Aqueous humor is produced at the ciliary body by a combination of passive and active mechanisms. The passive mechanism consists of ultrafiltration of fluid across the vessel wall in the microcirculation and produces a flux J_{uf} that is driven by trans-membrane differences in hydrostatic and oncotic pressures, the oncotic flux being mediated by a protein reflection coefficient σ_p, see Eq (1). The passive production mechanism is accounted for in the model through the filtration block (resistance and current generator in parallel) between the capillary node in the ciliary circulation (with pressure $P_{cl,c}$) and the node in the aqueous circuit (with pressure IOP), resulting in the flux J_{uf}.

The active mechanism is due to secretion of ions in the non-pigmented epithelium, which creates a difference in ionic concentration that draws fluid into the eye via osmosis [27]. Following [26, 52], we assume that the active secretion contributes with a constant flow rate, which is modeled in the electrical analogue of Fig 2 by the generator J_{secr}. Thus, J_{secr} is a model input and is listed in Table 3.

Table 3. Summary of model inputs.

Model Inputs		Baseline	Source
Arterial Pressure	P_A	92.0 mmHg	[24]
Venous Pressure	P_V	5.4 mmHg	[24]
CSF production rate	Q_{CF}	299.5 μl min^{-1}	[24]
Active secretion rate of aqueous humor	J_{secr}	6.9525 μl min^{-1}	[52] [26]

https://doi.org/10.1371/journal.pone.0216012.t003

The drainage of aqueous humor from the eye is driven by mechanical pressure differences and occurs through two different pathways: the trabecular pathway (also known as conventional), resulting in the flow J_{tm} and the uveoscleral pathway (also known as unconventional), resulting in the flow J_{uv}. Both are modeled as nonlinear resistors R_{tm} and R_{uv}, as in [26, 27, 53].

Since the system is assumed to be at steady state, aqueous inflow and outflow must be equal to each other, leading to the balance equation $J_{uf} + J_{secr} = J_{tm} + J_{uv}$. The full model of the eye results from coupling the circuits described above as shown in Fig 2. The coupling between the two circuits is truly two-ways: *(i)* the aqueous humor circuit influences the vascular circuit, since the IOP acts as an external pressure on the intraocular venules (see dashed cyan arrows in Fig 1), thereby influencing their resistances; *(ii)* the vascular circuit influences the aqueous humor circuit, since blood pressure in the ciliary body capillaries contributes to the production of aqueous humor.

Coupling of the eye and brain models

The connections between the eyes and brain models are marked with special symbols in Fig 1. Red filled circles denote connections between arterial compartments; blue filled circles those between venous compartments. Finally, the cyan and grey arrows indicate the pressures (intraocular and extraocular, respectively) that act on both sides of the lamina cribrosa in the optic nerve head and on the vessels. More precisely:

- the node corresponding to the ophthalmic artery (OA) the eye model (whose pressure is denoted as $P_{Eye,in}$ in Fig 1) is connected to the intracranial arteries in the brain model (whose pressure is denoted as P_I) through an effective vascular resistance ($R_{I,OA}$);
- the node corresponding to the cavernous sinus in the brain (whose pressure is denoted as $P_{Eye,out}$) and that corresponding to the episcleral veins in the eye (whose pressure is denoted as P_{evp}) are directly connected to the venous sinus in the brain model (whose pressure is denoted as P_S);
- the lamina is acted upon by the IOP from the ocular side (cyan arrow) and by the CSFp in the subarachnoid space in the optic nerve, here assumed to be equal to the extraventricular CSFp (grey arrow).

Thank to this coupling, this work presents the first model capable of simulating in a self-consistent manner the fluid-dynamic eye-brain-body connections as the result of *(i)* the pressure drop between the central arteries (P_A) and the central veins (P_V); *(ii)* the active secretion of aqueous humor in the eye (J_{secr}); and *(iii)* the production of CSF in the brain (Q_{CF}), as summarized in Table 3.

Simulation of microgravity conditions

In space, the human body experiences a series of changes in external conditions with respect to earth. The most obvious one is the lack of gravity that has an influence on the redistribution

of fluids within the body. In particular, a significant fluid shift has been observed from the lower to the upper body and head. This is thought to produce an increase in ICP and also a variation in the blood colloid osmotic pressure in the brain [1, 6, 54]. However, the effect of microgravity on ICP is quite complex. In acute zero gravity conditions simulated during parabolic flight, ICP during supine posture fell in microgavity relative to earth conditions and the removal of gravity was found to prevent the normal lowering of ICP when upright [55].

In the present paper, microgravity conditions are simulated following the same approach as in [24], namely: *(i)* we impose zero hydrostatic pressure distribution; *(ii)* we set the central venous pressure to zero; *(iii)* we decrease blood colloid osmotic pressure as a consequence of fluid shift towards the head; *(iv)* we weaken the blood-brain barrier by modifying the Starling-Landis equation coefficients (see Eq (1)). In particular, we increase the filtration coefficient K_{CB} between capillaries in the brain and the brain tissue and correspondingly decrease the reflection coefficient σ_{CB} as suggested by [24].

We also consider long head-down tilt (LHDT) conditions that are the most common earth clinical model used to mimic the effects of microgravity on body fluids shift. In particular, HDT is a ground-based experimental procedure, which simulates the effects of microgravity on the cardiovascular system: participants lay head down on a surface inclined by an angle θ = 6 degrees, with respect to a horizontal plane, and experience a shift of cephalic fluid similar to that occurring in microgravity. The position change affects the hydrostatic pressure distribution in the human body, which is equal to $\rho g x \sin\theta$, with x being an axis running along the body and centered in the right atrium, ρ is fluid density and g is the gravitational acceleration. This means that the pressure variation between the central and intracranial compartments in the model can be written as $G \sin\theta$, with $G = \rho g H$, and H is the distance between the right atrium and the base of the brain. We use our model to simulate LHDT, by changing both the gravitational direction and the blood oncotic pressure in the brain.

Summarizing, we simulate: *(i)* LHDT; *(ii)* microgravity environment with an intact blood/brain barrier (M0); and *(iii)* microgravity environment with a weakened blood/brain barrier (M1, M2), imposing the condition reported in Table 4.

We remark that a weakened blood/brain barrier was utilized in [24] to simulate microgravity conditions. However, recent studies showed that the ICP drop predicted in [24] without any dysfunction of the blood/brain barrier actually matched data collected during acute weightlessness in parabolic flight [55]. In this work, we opted for not ruling out completely the possibility of a dysfunctional blood/brain barrier, since there might be other factors, such as radiation exposure, which may compromise it during long space flights. Thus, in the following we will compare the model predictions obtained with intact (M0) and dysfunctional (M1, M2) barrier.

In all four cases, model simulations are performed for decreasing values of the blood oncotic pressure, corresponding to different degrees of fluid shift towards the upper part of the

Table 4. Conditions for simulated microgravity environment, as in [24].

	Simulation Conditions	
LHDT	$P_{A,LHDT} = P_A + G \sin\theta$	$P_{V,LHDT} = P_V + G \sin\theta$
	$K_{CB,LHDT} = 0.0665$ ml mmHg^{-1} min^{-1}	$\sigma_{CB,LHDT} = 1$
M0	$P_{A,M0} = P_A$	$P_{V,M0} = 0$
	$K_{CB,M0} = 0.0665$ ml mmHg^{-1} min^{-1}	$\sigma_{CB,M0} = 1$
M1	$P_{A,M1} = P_A$	$P_{V,M1} = 0$
	$K_{CB,M1} = 0.1164$ ml mmHg^{-1} min^{-1}	$\sigma_{CB,M1} = 0.5714$
M2	$P_{A,M2} = P_A$	$P_{V,M2} = 0$
	$K_{CB,M2} = 0.1330$ ml mmHg^{-1} min^{-1}	$\sigma_{CB,M2} = 0.5$

https://doi.org/10.1371/journal.pone.0216012.t004

body. Specifically, denoting by π_c the blood oncotic pressure, the oncotic pressure differences involved in the ultrafiltration of aqueous humor in the eye and CSF in the brain can be written as $\Delta\pi_p = \pi_c - \pi_{ah}$ and $\Delta\pi_{CB} = \pi_c - \pi_B$, respectively. Since $\pi_{ah} \approx 0$ mmHg [27, 52], a reasonable baseline value for π_c is 25 mmHg. Simulations are performed for $\pi_c \in (18.5, 25)$ mmHg. Decreases of 3.3 mmHg and 6.3 mmHg have been associated with LHDT and microgravity conditions, respectively, leading to π_c values of 21.7 mmHg and 18.7 mmHg, respectively [24], which are indeed included in the simulated interval.

Solution strategy

We implemented the circuit shown in Fig 1 in OpenModelica [56], which is a free, open-source modeling and simulation environment. In particular, we used the analogue electric components environment, which allows the user to draw a circuit and specify analytical expressions for nonlinear components. The circuit is automatically solved by the software. The graphic-oriented design of the circuit allows the user to easily modify the network and to include a large number of components.

Model calibration

The main goal of the model calibration is to select the values for all model parameters in such a way that, at baseline, the model predictions are in agreement with values reported in the literature. Since the choice of model parameters is one of the most delicate and important steps in devising a mathematical model, we report here the main rationale behind our choices. In the following, we denote reference values using overlined symbols.

We remark that, whenever possible we adopted, the same parameter values as those reported in the literature, as summarized in Table 5. In particular, considering posture, the brain model by Lakin et al [24] has been calibrated utilizing measurements pertaining to the supine position. The retinal model developed by some of the authors [25] has been calibrated utilizing measurements of blood velocity obtained via Color Doppler Imaging when the individual was resting on a reclined chair. Thus, we can assume that the reference for our model is the supine position.

Unfortunately, though, some parameters pertaining to blood flow resistances were not readily available in the literature and needed to be calibrated starting from reference values of flow rates and pressures. In this perspective, it is important to emphasize that experimental measurements of flow rates and pressures are influenced by many factors, including age [57–59], gender [60–62], posture [63–66] and time of the day [61, 67, 68], not to mention the instrument utilized for the measurement [69, 70] and the measurement protocol [7, 8]. Thus, it would be necessary to collect all the required data for model calibration simultaneously on the eyes and brain of a large cohort of individuals, at same time of the day, with consistency in the adopted instruments and measurement protocols. Such a dataset is currently not available and its realization would be a great contribution to advance the current knowledge in cardiovascular physiology in health and disease.

Reference values for blood flow rates in the eye. A reference value of $\overline{Q}_r = 40.9\mu\text{l/min}$ for retinal blood flow can be found in [25]. This value results from a review of the experimental measurements reported in [71–75]. Similarly, a reference value of $\overline{Q}_{cl} = 133\mu\text{l/min}$ for the blood flow in the ciliary body can be found in [76]. This value was estimated from measured levels of aqueous-to-plasma ascorbate ratio and aqueous production rate [77, 78] The choice of a reference value for the choroidal blood flow is less obvious due to the lack of experimental measurements. Here we choose a value of $\overline{Q}_{ch} = 368\mu\text{l/min}$, which is within the same range as

Table 5. Summary of model parameters.

Model Parameters		
Brain		
Cerebral Blood Flow		
R_I	$33.5 \cdot 10^{-3}$ mmHg min ml^{-1}	[24]
R_C	$12.7 \cdot 10^{-3}$ mmHg min ml^{-1}	[24]
R_S	$12.7 \cdot 10^{-3}$ mmHg min ml^{-1}	[24]
Cerebrospinal and Interstitial Fluid Flow		
K_{CB}	0.0665 ml mmHg^{-1} min^{-1}	[24]
σ_{CB}	1	[24]
$\Delta\pi_{CB}$	21 mmHg	[24]
R_{BT}	1.55 mmHg min ml^{-1}	[24]
R_{FT}	0.6678 mmHg min ml^{-1}	[24]
R_{FB}	0.9023 mmHg min ml^{-1}	[24]
R_{TS}	9.90 mmHg min ml^{-1}	[24]
Eye		
Blood Flow		
E_v	495 mmHg	[25]
h_v	$7.73 \cdot 10^{-4}$ cm	this work
μ_v	$2.12 \cdot 10^{-5}$ mmHg · s	this work
ν_v	0.49	[25]
$\mathcal{L}_v$	0.80 cm	this work
$R_{cl,in}$	16.70 mmHg min ml^{-1}	this work
$R_{cl,a1} = R_{cl,a2}$	105.26 mmHg min ml^{-1}	this work
$R_{cl,c1} = R_{cl,c2}$	33.83 mmHg min ml^{-1}	this work
$\mathcal{A}_{cl,v}$	$2.61 \cdot 10^{-4}$ cm^2	this work
$R_{cl,out}$	23.90 mmHg min ml^{-1}	this work
$R_{cra,in}$	376.76 mmHg min ml^{-1}	this work
$\mathcal{L}_{cra,1} = \mathcal{L}_{cra,2}$	0.44 cm	[25]
$\mathcal{L}_{cra,3}$	0.02 cm	[25]
$\mathcal{L}_{cra,4}$	0.1 cm	[25]
$\mathcal{D}_{cra}$	$175 \cdot 10^{-4}$ cm	[25]
E_{cra}	2250 mmHg	[25]
h_{cra}	$4 \cdot 10^{-3}$ cm	[25]
μ_{cra}	$2.25 \cdot 10^{-5}$ mmHg · s	[25]
ν_{cra}	0.49	[25]
$R_{r,a1} = R_{r,a2}$	101 mmHg min ml^{-1}	this work
$R_{r,c1} = R_{r,c2}$	94.33 mmHg min ml^{-1}	this work
$\mathcal{A}_{r,v}$	$1.55 \cdot 10^{-4}$ cm^2	this work
$\mathcal{L}_{crv,1}$	0.1 cm	[25]
$\mathcal{L}_{crv,2}$	0.02 cm	[25]
$\mathcal{L}_{crv,3} = \mathcal{L}_{crv,4}$	0.44 cm	[25]
$\mathcal{D}_{crv}$	$238 \cdot 10^{-4}$ cm	[25]
E_{crv}	4500 mmHg	[25]
h_{crv}	$10.7 \cdot 10^{-4}$ cm	[25]
μ_{crv}	$2.43 \cdot 10^{-5}$ mmHg· s	[25]
ν_{crv}	0.49	[25]
$R_{crv,out}$	247.25 mmHg min ml^{-1}	this work

(*Continued*)

Table 5. (Continued)

Model Parameters		
$R_{ch,in}$	6.04 mmHg min ml^{-1}	this work
$R_{ch,a1} = R_{ch,a2}$	38.12 mmHg min ml^{-1}	this work
$R_{ch,c1} = R_{ch,c2}$	12.25 mmHg min ml^{-1}	this work
$\mathcal{A}_{ch,v}$	5.06 ·10^{-4} cm^2	this work
$R_{ch,out}$	8.66 mmHg min ml^{-1}	this work
Aqueous Humour		
L_{in}	0.3 μl min^{-1} mmHg^{-1}	[52]
σ_p	1	[52]
$\Delta\pi_p$	25 mmHg	[52]
k_1	0.4 μl min^{-1}	[27]
k_2	5 mmHg	[27]
R_0	2.2 mmHg min μl^{-1}	[53]
κ	0.012 mmHg^{-1}	[53]
Body-Brain-Eye Coupling		
R_A	101.5 mmHg min ml^{-1}	[24]
R_V	407.99 mmHg min ml^{-1}	[24]
R_{TV}	52.38 mmHg min ml^{-1}	[24]
$R_{I,OA}$	18.27 mmHg min ml^{-1}	this work

https://doi.org/10.1371/journal.pone.0216012.t005

the findings reported in [79] obtained using Magnetic Resonance Imaging, while yielding a percent ratio between retinal and choroidal blood flow of 10% to 90% as indicated in [15].

Reference values for blood pressures in the eye. A reference value of $\overline{P}_{Eye,in} = 62.2$ mmHg for blood pressure at the level of the ophthalmic artery can be found in [25]. As suggested by the measurements performed via ophthalmomanometry-Doppler in [80], this value can be estimated as $\overline{P}_{Eye,in} = 2/3\,\overline{\mathrm{MAP}}$, where $\overline{\mathrm{MAP}}$ is the reference value for the mean arterial pressure defined as $\overline{\mathrm{MAP}} = 1/3\,\overline{\mathrm{SBP}} + 2/3\,\overline{\mathrm{DBP}}$, with $\overline{\mathrm{SBP}}$ and $\overline{\mathrm{DBP}}$ denoting the reference values for systolic and diastolic blood pressures, here set at 120 mmHg and 80 mmHg, respectively. A reference value of $\overline{P}_{Eye,out} = 8$ mmHg for blood pressure at the venous output of the eye can be found in [27]. This value is considered as a representative mean value among the wide range of measurements reported in the literature, as reviewed in [81]. References values for the pressure distribution inside the circuit for the retinal circulation have been computed using the mathematical model presented in [25]. Reference values of $\overline{P}_{cl,in} = 60$ mmHg and $\overline{P}_{cl,v} = 17$ mmHg can be found in [27]. These values were obtained indirectly from estimates of blood volume and vascular compliance. A reference value of 32 mmHg for the pressure between arterioles and capillaries can be found in [46]. This value is based on the choice adopted in [82], which was based on previous modeling and experimental work [83–85]. Reference values for the pressures within the choroidal circulation have been set as to mirror those in the ciliary circulation, as in [27].

Reference values for vascular resistances in the eye. Given the reference values of flow rates and pressures, the values for vascular resistances can be found by means of Ohm's law. The parameters involved in the calculation of the vascular resistances pertaining to CRA and CRV follow directly from the work by [25]. For what concerns the parameters involved in the resistances for retinal venules, we follow the same approach as in [25], where a dichotomous network model for the retinal circulation proposed in [86] was used to define the hierarchical architecture of the venous retinal segment, leading to the parameter values reported in Table 6.

Table 6. Baseline values for pressures and flow rates under physiological condition.

	Baseline values			
	Pressures	(mmHg)	Flow rates	(ml min^{-1})
Brain				
	P_I	81.9956	Q_{IC}	1035
	P_C	34.1543	Q_{CB}	0.1291
	P_S	7.8210	Q_{FT}	0.3004
	P_B	11.2125	Q_{FB}	$42.42 \cdot 10^{-3}$
	P_F	11.2125	Q_{BT}	0.1287
			Q_{TS}	0.3220
			Q_{CS}	1034.5
Eye				
	$P_{cra,in}$	46.833	Q_r	$40.9 \cdot 10^{-3}$
	$P_{cra,1}$	43.9041	Q_{ch}	$367.9 \cdot 10^{-3}$
	$P_{cra,2}$	40.9753	Q_{cl}	$135.7 \cdot 10^{-3}$
	$P_{cra,3}$	40.8465	J_{uf}	$-3.7 \cdot 10^{-3}$
	$P_{cra,4}$	40.2141	J_{ah}	$3.3 \cdot 10^{-3}$
	$P_{r,a}$	36.0875	J_{uv}	$2.9983 \cdot 10^{-4}$
	$P_{r,c}$	28.1062	J_{tm}	0.003
	$P_{r,v}$	22.1371		
	$P_{crv,1}$	20.0226		
	$P_{crv,2}$	19.8107		
	$P_{crv,3}$	19.7729		
	$P_{crv,4}$	18.8452		
	$P_{crv,out}$	17.9235		
	$P_{ch,in}$	60.003		
	$P_{ch,a}$	45.9777		
	$P_{ch,c}$	27.4443		
	$P_{ch,v}$	16.9714		
	$P_{ch,out}$	11.0069		
	$P_{cl,in}$	60.0213		
	$P_{cl,a}$	46.1248		
	$P_{cl,c}$	27.7616		
	$P_{cl,v}$	17.118		
	$P_{cl,out}$	11.0651		
	P_{LC}	0		
	IOP	14.9662		
	P_{evp}	7.82104		
Body-Brain-Eye Coupling				
	$P_{Eye,in}$	62.2270	Q_A	1035
	P_T	11.0119	Q_{TV}	0.1071
	$P_{Eye,out}$	7.8210	$Q_{CvS} = Q_{Eye,out}$	0.5475
	$RLTp$	11.0119	Q_{SV}	1035
			$Q_{OA} = Q_{Eye,in}$	0.5407
			Q_V	1035

https://doi.org/10.1371/journal.pone.0216012.t006

Owing to lack of data concerning ciliary and choroidal circulations, we assumed that all the elastic parameters are the same as those for the retina. For what concerns characteristic areas and lengths, we reasoned as follows. Let the blood volumes in the venous segments of retinal ciliary body and choroidal circulations be defined as $\mathcal{V}_{i,v} = \mathcal{A}_{i,v}\mathcal{L}_{i,v}$, for $i = r, cl, ch$. Let us

assume that the ratio between blood volumes in the retinal and ciliary body (res. choroidal) venous segment is that same as the ratio between the corresponding flow rates, namely

$$\frac{\mathcal{V}_{i,v}}{\mathcal{V}_{r,v}} = \frac{\overline{Q}_i}{\overline{Q}_r}, \quad i = cl, ch. \tag{6}$$

Then it follows that

$$\mathcal{V}_{i,v} = \mathcal{A}_{i,v}\mathcal{L}_{i,v} = \frac{\overline{Q}_i}{\overline{Q}_r}\mathcal{V}_{r,v}, \tag{7}$$

which implies that

$$\mathcal{L}_{i,v} = \frac{\overline{Q}_i}{\overline{Q}_r}\frac{\mathcal{V}_{r,v}}{\mathcal{A}_{i,v}} \quad i = cl, ch. \tag{8}$$

The value of $\mathcal{A}_i$, $i = cl, ch$, is computed imposing that, when $\overline{\Delta p}_t = \overline{P}_{i,v} - \overline{IOP}$, with $\overline{IOP} = 15$ mmHg, the value of the resistance in the Starling model equals the value of $\overline{R}_{i,v1} + \overline{R}_{i,v2}$ obtained using Ohm's law.

The solution of the system obtained for the model parameters reported in Table 5 leads to the baseline distribution of pressures and flow rates reported in Table 6. A thorough validation of the model is the object of the next section.

Model validation

The mathematical model presented here connects numerous blocks that have been developed independently by different authors. Thus, the validation of each block considered individually has been addressed in different articles. Specifically, for the circulation in the retina and in the central retinal vessels we refer to [25], for the circulation in the ciliary body and in the choroid we refer to [49] and [27], for the aqueous humor circulation we refer to [26] and for the cerebral circulation of blood, interstitial fluid and CSF we refer to [24]. The validation of the modeling assumptions concerning the connections between the various components has been presented at the 2018 Annual Meeting of the Association for Research in Vision and Ophthalmology [13, 14]. The model proved capable of capturing a slight increase in IOP following an increase in blood pressure, consistently with the findings of the Rotterdam study [87], the Blue Mountains eye population-based study [88] and the Beijing eye study [89]. The model also predicted a decrease in CSFp with blood pressure, consistently with the findings of Ren et al reported in [90]. In addition, the model confirmed that the pressure in the vortex veins before they exit the sclera is approximately equal to the IOP over a wide range of values, as reported by Bill in [91]. These validation results are quite impressive, considering that these studies were not used for model calibration. The successful validation of the model blocks considered separately [24–27, 49] and jointly [13] supports the utilization of the model to study the physiological connections between ocular and cerebral fluid flows.

Results and discussion

We now turn to the discussions of the results obtained by simulating microgravity conditions using the mathematical model presented in the previous sections. We consider the four different cases summarized in Table 4, namely LHDT, M0, M1 and M2.

Changes in the blood oncotic pressure modify both $\Delta\pi_{CB}$ and $\Delta\pi_p$, leading to changes in the filtration across the blood-brain barrier and the ciliary body, respectively, and, consequently,

to changes in ICP, CSFp and IOP. This is a crucial ingredient to interpret the results of the model. We also note that the model is highly nonlinear and, in particular, the Starling resistors in the venous segments of the eye are likely to play an important role. Specifically, when the transmural pressure becomes negative the venous compartments collapse, giving rise to a significant increase in resistance, according to Eq (4).

Fig 4 shows IOP (cyan), ICP (grey) and the radial stress acting on *cra* and *crv* (green) as a function of the blood oncotic pressure π_c for the four cases of interest (LHDT, M0, M1 and M2). We recall that a reasonable baseline value for π_c on earth is ≈ 25 mmHg, which may decrease to 21.7 mmHg in LHDT and to 18.7 mmHg in microgravity conditions. These reference values are indicated with dashed lines in the corresponding figures.

In all cases reported in Fig 4, and in agreement with the results of [24], the intracranial pressure grows as π_c decreases and the increase is more marked when the weakening of the blood/brain barrier is accounted for (M1 and M2). The ICP variation is approximately linear with π_c.

IOP also grows as the oncotic pressure difference decreases. In the Starling resistors, collapse of the flexible pipes depends on the transmural pressure that, in all cases but the prelaminar *crv*, is given by the difference between the intraluminal pressure and the IOP. Therefore, a growth in IOP can lead to vessel collapse. Since this is an important ingredient in the model, in Fig 4 we report with coloured dotted lines the values of π_c at which each of the compartments collapses. Throughout this section, we use consistently the following *color code* to identify different ocular blood compartments:

- black for retinal circulation;
- red for choroidal circulation; and
- blue for ciliary body circulation.

Thus, for example, black vertical lines in Fig 4 indicate the maximum value of π_c for which vessel collapse in the retinal circulation occurs. In all considered cases, the first compartment to collapse (for the largest values of π_c) is that corresponding to the ciliary venules. Soon afterwards, and further decreasing π_c, the choroidal venules and the postlaminar *crv* also collapse. Finally, the prelaminar *crv* collapses at a slightly smaller value of π_c. This last event is triggered by a compressive radial stress acting on the vessel, produced by the lamina deformation. We note that all these events occur in a relatively narrow range of values of the blood oncotic pressure π_c and, approximately, at the same values of π_c in all considered cases. In the case of LHDT the collapse is slightly delayed.

We now analyze in detail the variation of the IOP with π_c shown in Fig 4 and discuss its implications for blood fluxes in the various ocular compartments. For the sake of clarity we will consider first the case of LHDT and then compare it with the microgravity cases (M0, M1 and M2). In Fig 4(a) the IOP varies almost linearly with π_c, in the range 20 mmHg $\lessapprox \pi_c \leq 25$ mmHg and, for $\pi_c \lessapprox 20$ mmHg, the dependency becomes markedly nonlinear. This change in behavior is related to the collapse of ciliary venules that occurs when the transmural pressure in the ciliary venules becomes negative. The collapse of the venules produces a pressure increase in the ciliary body capillaries and arterioles. This increases the aqueous production rate and, in turn, makes the IOP grow. Finally, we note that the radial stress in the lamina cribriosa remains almost constant over a wide range of values of π_c and then sharply increases.

The fluxes in the retina, choroid and ciliary body circulation systems, normalized with their respective baseline values, are reported in Fig 5. The figure shows that, as π_c decreases, the ciliary and choroidal fluxes decrease almost linearly until vessel collapse occurs, and then do so much more rapidly. Interestingly, a different behavior is predicted by the model for the

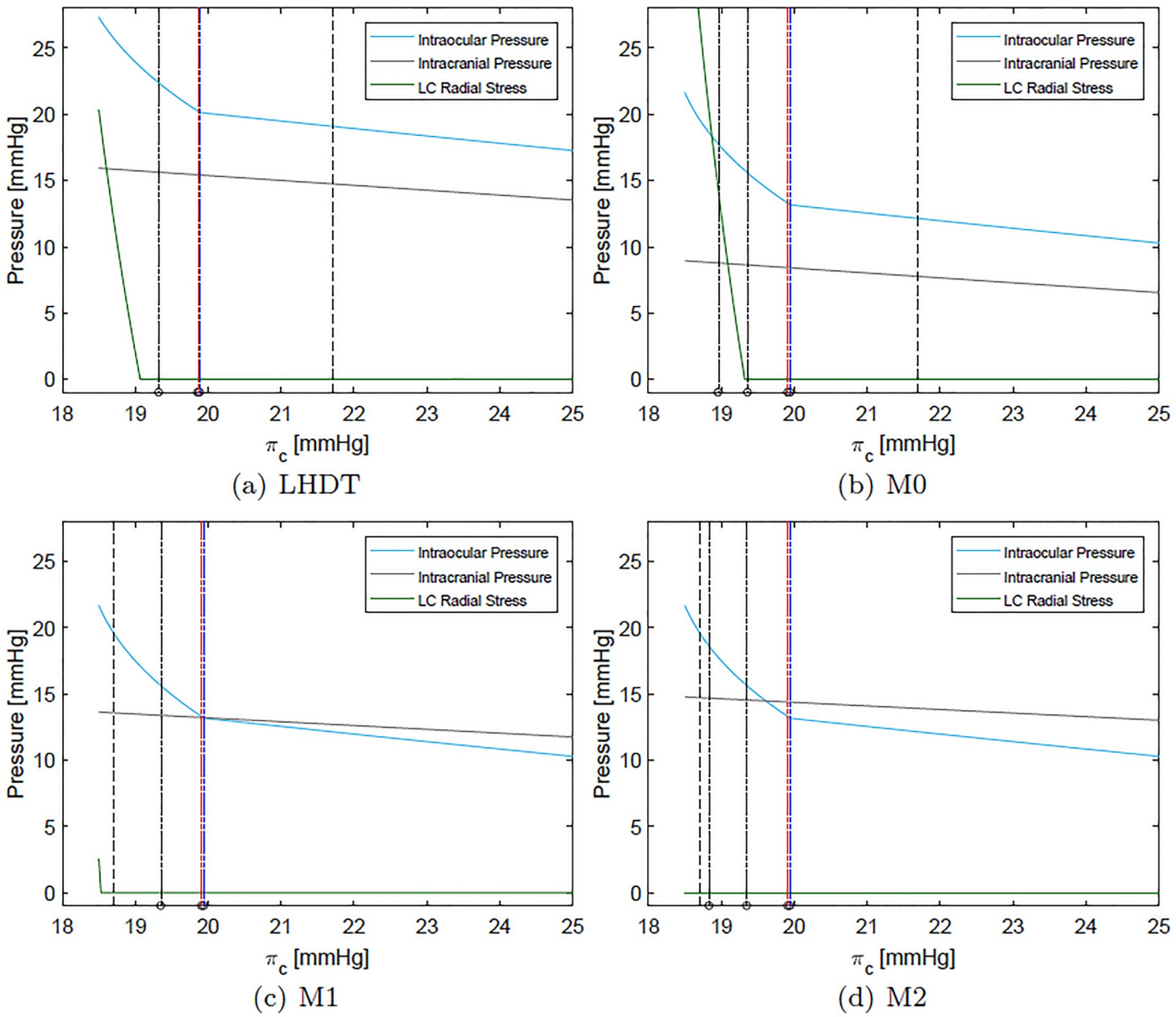

Fig 4. Intraocular, intracranial and compressive radial stress within the lamina cribrosa (LC) as a function of the blood oncotic pressure in capillaries π_c. The physiological value of π_c on earth is ≈ 25 mmHg. The vertical dotted line indicates the value of π_c representative of each case. Dashed coloured vertical lines indicate the values of π_c at which each of compartment collapses (black for central retinal vein, red for choroidal venules and blue for ciliary venules). Panel (d) appeared in [12].

https://doi.org/10.1371/journal.pone.0216012.g004

retina. Over a wide range of values of π_c and before venules collapse happens, the flux in the retina remains almost constant. This suggests that the particular architecture of the retinal vasculature provides a sort of mechanical (i.e. purely passive) blood flow regulation in response to IOP changes. This behavior was already observed in [25], who proposed a model of the retinal circulation alone. It is interesting to find that this feature is maintained by the full coupled, interconnected model. When venules collapse in the ciliary body and choroidal circulation, the flux in the retina initially grows. This is due to the fact that the retinal circuit is arranged in

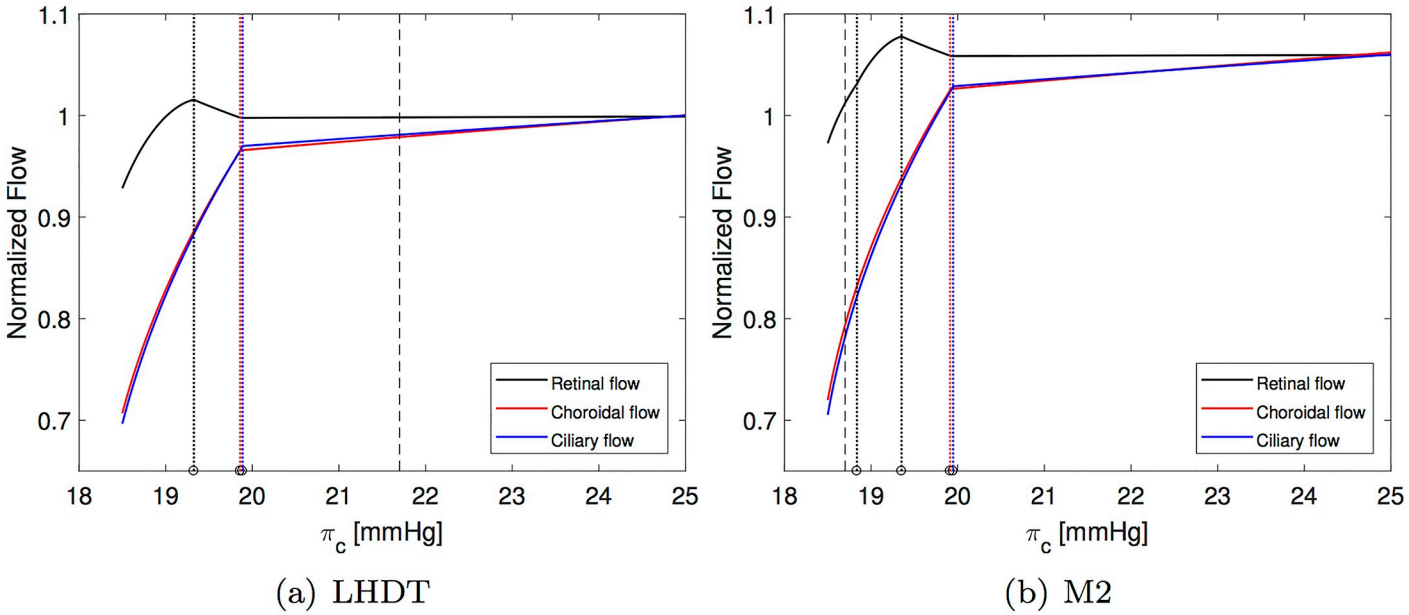

Fig 5. Normalized fluxes in the retina, choroid and ciliary body as a function of the blood oncotic pressure in capillaries π_c. All fluxes are normalized with their respective baseline value. The vertical dashed line indicates the value of π_c representative of each case. Dotted colored vertical lines indicate the values of π_c at which each of compartment collapses (black for central retinal vein, red for choroidal venules and blue for ciliary venules). Panel (b) appeared in [12].

https://doi.org/10.1371/journal.pone.0216012.g005

parallel to the other vascular beds and a decrease in flux in the ciliary body and choroid is partially compensated by an increase in the retinal blood flow. Once the *crv* also collapses, blood flow in the retina starts to drop significantly.

Figs 6 and 7 show the dependency of the transmural pressure in various compartments on the blood oncotic pressure π_c. All the plots can be interpreted in the light of the comments above and provide a detailed picture of pressure changes in the ocular circulation as a response to the LHDT experiment.

Finally, the LHDT case is compared with the simulations of microgravity conditions. Fig (4b)–(4d) shows that in microgravity conditions the ICP is smaller than in the case of LHDT, when the effect of blood/brain barrier disruption is not accounted for. ICP increases as the filtration and reflection coefficients are changed. These results are in agreement with the findings of [24]. The IOP predicted by our model is invariably lower in the cases of microgravity than of LHDT, even if it is larger than in physiological earth conditions. The effect of the blood/brain barrier integrity is far less important for the IOP than it is for the intracranial pressure. It is noted that in Figs 6 and 7 we only report the curves corresponding to the case M2, since they are almost coincident with those relative to the cases M0 and M1. Concerning blood fluxes, the dependency on π_c is similar to the LHDT case. However, the flux can be higher than in baseline earth conditions, especially in the retina. This is essentially due to the lowering of the central venous pressure.

Changes in IOP associated with prolonged head tilt have also been measured experimentally. In a LHDT study involving 16 healthy subjects, Taibbi et al found pre- and post-bed IOP values to be approximately 13 mmHg when measured via iCare (Icare Finland Oy, Espoo, Finland), with an increase of 2.13 and 1.74 mmHg in the right and left eye, respectively, at ten days into bed rest [92]. In another study, Taibbi et al observed that the iCare measurements of IOP increased of 1.42 mmHg and 1.79 mmHg from baseline during 14- and 70-day LHDT studies, respectively [7]. Baseline IOP values for the 16 subjects in the 14 day LHDT study and for the 6 subjects in the 70 day LHDT study ranged within 11.91–15.66 mmHg and 10.15–

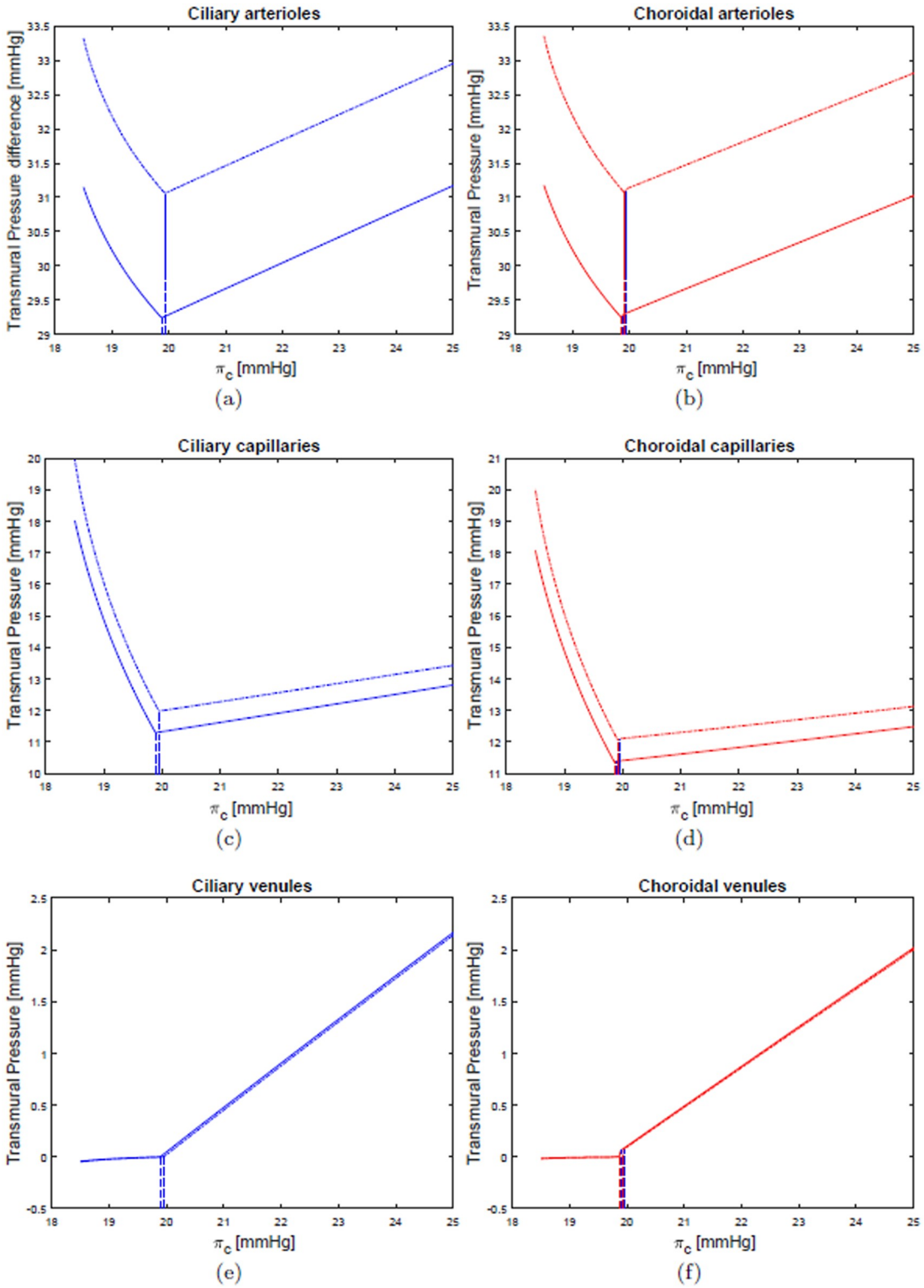

Fig 6. Transmural pressures in various compartments of the ciliary and choroidal circulations. LHDT solid line, M2 dash-dotted line.

https://doi.org/10.1371/journal.pone.0216012.g006

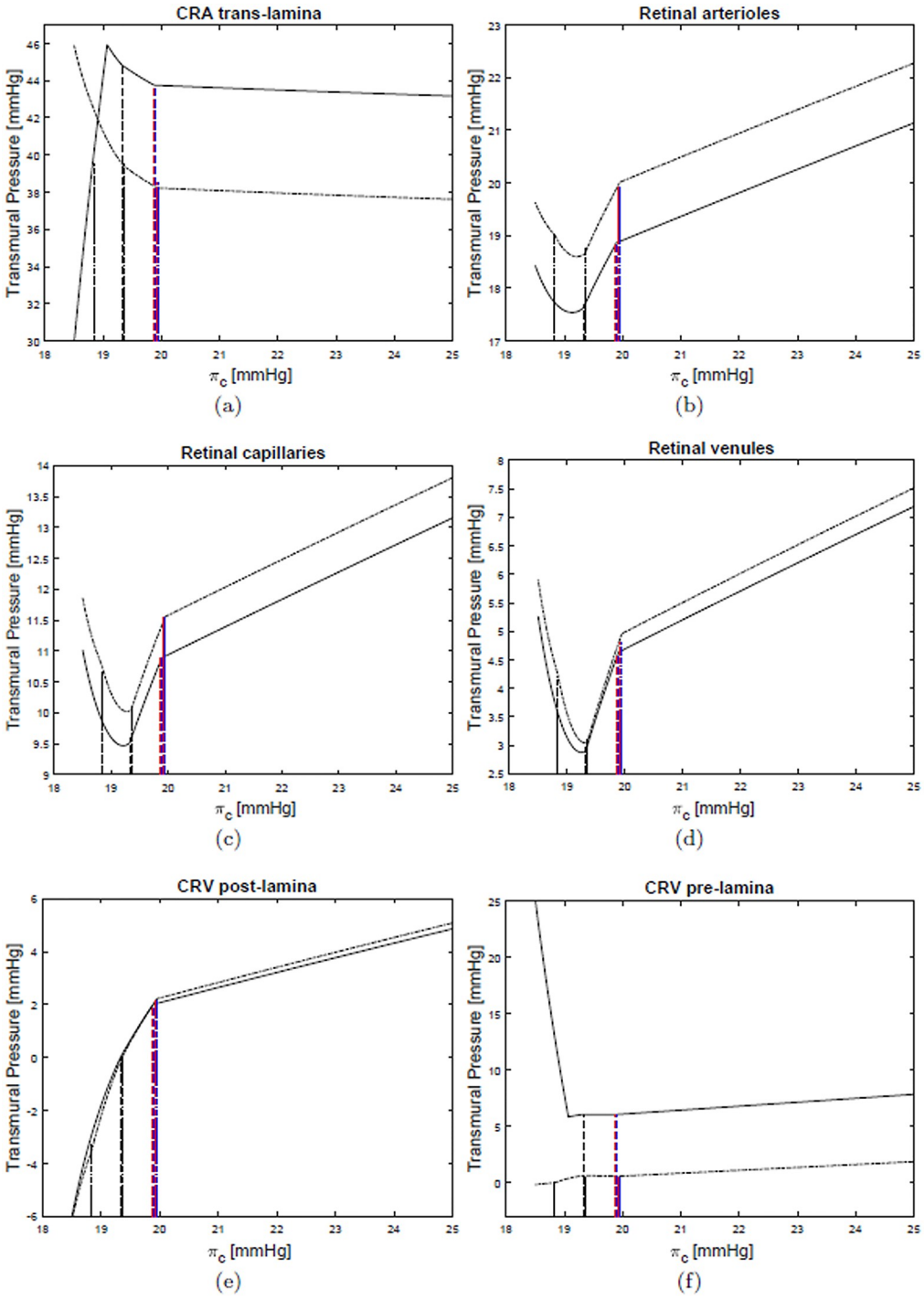

Fig 7. Transmural pressures in various compartments of the retinal circulation. LHDT solid line, M2 dash-dotted line.

https://doi.org/10.1371/journal.pone.0216012.g007

16.27 mmHg, respectively. IOP values predicted by our model in the LHDT case are on the higher end with respect to those reported in experimental studies, even though the predicted IOP increases are of the same order of magnitude as those measured experimentally. Specifically, as π_c is decreased from 25 to 20 mmHg, our model predicts an IOP increase from

approximately 17.5 to 20 mmHg. Considering that our model does not include any regulatory mechanism, these results are quite satisfactory.

Conclusion

In this paper, a lumped parameter model of fluid flow in the eyes and brain is proposed to study the flow of blood, interstitial fluid, CSF and aqueous humor. Despite its many limitations, including the fact that time-dependence and vascular regulation are not accounted for, the model proved capable of simulating the relationships among IOP, CSFp and blood pressure reported in major clinical and population-based studies, as reported in [13]. In addition, the model is able to capture the relationship between choroidal venous pressure and IOP reported in the seminal work by Bill in 1963 [91], thereby suggesting that it may prove instrumental to study blood outflow through the vortex veins, which is thought to play a very important role in many pathologies but remains very difficult to measure [13].

The model has been utilized to investigate changes in flow and pressure distributions associated with long term exposure to microgravity conditions. In this respect our model is complementary to the one proposed in [9], which was focused on the short term effects induced by acute gravitational variations. Simulation results point at a purely mechanical feedback mechanism due to the collapsibility of the retinal venules exposed to IOP that would help maintain a relatively constant level of blood flow through the retina despite microgravity-induced changes in pressure. Thus, a certain level of regulation is achieved in the retina even though active regulatory mechanisms are not included in the model. Interestingly, a similar mechanism is not present in the choroid and ciliary body due to their different vascular architectures. We hypothesize that this mechanism may offer additional protection to the retinal vasculature when exposed to extreme conditions, such as those associated with long space flights [2]. It is important to notice that various conditions during space flight are thought to alter vascular regulatory capabilities, particularly the increased amount of CO_2 in the air. With this in mind, a purely passive regulatory mechanism, as that predicted by the model for the retinal circulation, might turn out to be of great importance to avoid retinal damages in space.

Thanks to its ability to self-consistently compute IOP and CSFp given a certain level of blood pressure, the model developed in this paper might also bear a great relevance for other pathologies beyond SANS, most importantly glaucoma. In addition, the ability to simulate the flow conditions in the venous segments of the eye is a major contribution in ophthalmology, since the veins are known to play a very important role in ocular physiology but are very difficult to measure in vivo.

We conclude by emphasizing that the model indeed includes a large number of parameters, which required careful calibration. Despite the very good results obtained on the model validation, it would be important to perform a sensitivity analysis on the paramater space to better assess the robustness of the model and direct its future extensions.

Acknowledgments

This work has been partially supported by the award NSF DMS-1853222/1853303, the Chair Gutenberg funds of the Cercle Gutenberg (France) and the Labex IRMIA and the IdEx Unistra (University of Strasbourg, France).

Author Contributions

Conceptualization: Fabrizia Salerni, Rodolfo Repetto, Alon Harris, Peter Pinsky, Marcela Szopos, Giovanna Guidoboni.

Formal analysis: Marcela Szopos, Giovanna Guidoboni.

Funding acquisition: Giovanna Guidoboni.

Investigation: Peter Pinsky, Marcela Szopos, Giovanna Guidoboni.

Methodology: Marcela Szopos, Giovanna Guidoboni.

Software: Fabrizia Salerni, Christophe Prud'homme, Marcela Szopos, Giovanna Guidoboni.

Supervision: Rodolfo Repetto, Alon Harris, Christophe Prud'homme, Marcela Szopos, Giovanna Guidoboni.

Validation: Fabrizia Salerni, Alon Harris, Marcela Szopos, Giovanna Guidoboni.

Visualization: Fabrizia Salerni, Christophe Prud'homme, Marcela Szopos, Giovanna Guidoboni.

Writing – original draft: Fabrizia Salerni, Rodolfo Repetto, Marcela Szopos, Giovanna Guidoboni.

Writing – review & editing: Christophe Prud'homme, Marcela Szopos, Giovanna Guidoboni.

References

1. National Aeronautics and Space Administration. Evidence Report. Risk of Spaceflight Associated Neuro-ocular Syndrome (SANS). Nov 30; 2017. https://humanresearchroadmap.nasa.gov/evidence/reports/SANS.pdf.
2. Nelson ES, Mulugeta L, Myers JG. Microgravity-induced fluid shift and ophthalmic changes. Life. 2014 Nov 7; 4(4):621–665. https://doi.org/10.3390/life4040621 PMID: 25387162
3. Seedhouse E. Microgravity and vision impairments in astronauts. Springer International Publishing; 2015.
4. Mader TH, Gibson CR, Pass AF, Kramer LA, Lee AG, Fogarty J, Tarver WJ, Dervay JP, Hamilton DR, Sargsyan A, Phillips JL, Tran D, Lipsky W, Choi J, Stern C, Kuyumjian R, Polk JD. Optic disc edema, globe flattening, choroidal folds, and hyperopic shifts observed in astronauts after long-duration space flight. Ophthalmology. 2011 Oct; 118(10):2058–2069. https://doi.org/10.1016/j.ophtha.2011.06.021 PMID: 21849212
5. Blomqvist CG, Nixon JV, Johnson RL Jr, Mitchell JH. Early cardiovascular adaptation to zero gravity simulated by head-down tilt. Acta Astronaut. 1980 Apr-May; 7(4-5):543–553. https://doi.org/10.1016/0094-5765(80)90043-0 PMID: 11541656
6. Parazynski SE, Hargens AR, Tucker B, Aratow M, Styf J, Crenshaw A. Transcapillary fluid shifts in tissues of the head and neck during and after simulated microgravity. J Appl Physiol. 1991 Dec; 71 (6):2469–2475. https://doi.org/10.1152/jappl.1991.71.6.2469 PMID: 1778948
7. Taibbi G, Cromwell RL, Zanello SB, Yarbough PO, Ploutz-Snyder RJ, Godley BF, Vizzeri G. Ocular outcomes comparison between 14-and 70-day head-down-tilt bed rest. Invest Ophthalmol Vis Sci. 2016 Feb; 57(2):495–501. https://doi.org/10.1167/iovs.15-18530 PMID: 26868753
8. Laurie SS, Macias BR, Dunn JT, Young M, Stern C, Lee SMC, Stenger MB. Optic disc edema after 30 days of strict head-down tilt bed rest. Ophthalmology. 2019 Mar; 126(3):467–468. https://doi.org/10.1016/j.ophtha.2018.09.042 PMID: 30308219
9. Nelson ES, Mulugeta L, Feola A, Raykin J, Myers JG, Samuels BC, Ethier CR. The impact of ocular hemodynamics and intracranial pressure on intraocular pressure during acute gravitational changes. J Appl Physiol. 2017 Aug 1; 123(2):352–363 https://doi.org/10.1152/japplphysiol.00102.2017 PMID: 28495842
10. Vera J, Mulugeta L, Nelson ES, Raykin J, Feola A, Gleason R, Samuels B, Myers JG. Lumped parameter models of the central nervous system for VIIP research. NASA Human Research Program Investigators Workshop; 13-15 Jan. 2015; Galveston, TX; United States.
11. Salerni F. Design and development of a mathematical model to analyse visual impairment in astronauts. Master Thesis, Universitá degli Studi di Genova (Italy) 2016.
12. Salerni F, Repetto R, Harris A, Pinsky P, Prud'homme C, Szopos M, Guidoboni G. Mathematical modeling of ocular and cerebral hemo-fluid dynamics: application to VIIP. Journal for Modeling in Ophthalmology. 2018; 2(2):64–68.

13. Guidoboni G, Salerni F, Repetto R, Szopos M, Harris A. Relationship between intraocular pressure, blood pressure and cerebrospinal fluid pressure: a theoretical approach. Invest Ophthalmol Vis Sci. 2018; 59(9):1665.
14. Guidoboni G, Salerni F, Repetto R, Szopos M, Harris A. Relationship between intraocular pressure, blood pressure and cerebrospinal fluid pressure: a theoretical approach. Journal for Modeling in Ophthalmology. 2019. In Press.
15. Weinreb RN, Harris A. Ocular blood flow in glaucoma. The 6th consensus report of the World Glaucoma Association. Kugler Publications; 2009.
16. Harris A, Siesky B, Zarfati D, Haine CL, Catoira Y, Sines DT, McCranor L, Garzozi HJ. Relationship of cerebral blood flow and central visual function in primary open-angle glaucoma. J Glaucoma. 2007 Jan; 16(1):159–163. https://doi.org/10.1097/01.ijg.0000212290.08540.93 PMID: 17224767
17. Harris A, Siesky B, Wirostko B. Cerebral blood flow in glaucoma patients. J Glaucoma. 2013 Jun-Jul; 22 Suppl 5:S46–S48. https://doi.org/10.1097/IJG.0b013e3182934b6b PMID: 23733128
18. Caprioli J, Coleman AL. Blood pressure, perfusion pressure, and glaucoma. Am J Ophthalmol. 2010 May; 149(5):704–712. https://doi.org/10.1016/j.ajo.2010.01.018 PMID: 20399924
19. Leske MC. Open-angle glaucoma—an epidemiologic overview. Ophthalmic Epidemiol. 2007 Jul-Aug; 14(4):166–172. https://doi.org/10.1080/09286580701501931 PMID: 17896292
20. Burgoyne CF. A biomechanical paradigm for axonal insult within the optic nerve head in aging and glaucoma. Exp Eye Res. 2011 Aug; 93(2):120–132. https://doi.org/10.1016/j.exer.2010.09.005 PMID: 20849846
21. Ren R, Zhang X, Wang N, Li B, Tian G, Jonas JB. Cerebrospinal fluid pressure in ocular hypertension. Acta Ophthalmol. 2011 Mar; 89(2):e142–148. https://doi.org/10.1111/j.1755-3768.2010.02015.x PMID: 21348961
22. Costa VP, Harris A, Anderson D, Stodtmeister R, Cremasco F, Kergoat H, Lovasik J, Stalmans I, Zeitz O, Lanzl I, Gugleta K, Schmetterer L. Ocular perfusion pressure in glaucoma. Acta Ophthalmol. 2014 Jun; 92(4):e252–266. https://doi.org/10.1111/aos.12298 PMID: 24238296
23. Gross JC, Harris A, Siesky BA, Sacco R, Shah A, Guidoboni G. Mathematical modeling for novel treatment approaches to open-angle glaucoma. Expert Rev Ophthalmol. 2017 Nov 2; 12(6):443–55. https://doi.org/10.1080/17469899.2017.1383896
24. Lakin WD, Stevens SA. Modelling the response of intracranial pressure to microgravity environments. Aspects of Mathematical Modelling. Eds: Hosking RJ, Venturino E. Springer-Birkhäuser Basel; 2008: 211–227.
25. Guidoboni G, Harris A, Cassani S, Arciero J, Siesky B, Amireskandari A, Tobe L, Egan P, Januleviciene I, Park J. Intraocular pressure, blood pressure, and retinal blood flow autoregulation: a mathematical model to clarify their relationship and clinical relevance. Invest Ophthalmol Vis Sci. 2014 May 29; 55 (7):4105–4118. https://doi.org/10.1167/iovs.13-13611 PMID: 24876284
26. Szopos M, Cassani S, Guidoboni G, Prud'homme C, Sacco R, Siesky B, Harris A. Mathematical modeling of aqueous humor flow and intraocular pressure under uncertainty: towards individualized glaucoma management. Journal for Modeling in Ophthalmology. 2016; 2(1):29–39.
27. Kiel JW, Hollingsworth M, Rao R, Chen M, Reitsamer HA. Ciliary blood flow and aqueous humor production. Prog Retin Eye Res. 2011 Jan; 30(1):1–17. https://doi.org/10.1016/j.preteyeres.2010.08.001 PMID: 20801226
28. Lakin WD, Stevens SA, Tranmer BI, Penar PL. A whole-body mathematical model for intracranial pressure dynamics. J Math Biol. 2003 Apr; 46(4):347–383. https://doi.org/10.1007/s00285-002-0177-3 PMID: 12673511
29. Goriely A, Geers MG, Holzapfel GA, Jayamohan J, Jérusalem A, Sivaloganathan S, Squier W, van Dommelen JA, Waters S, Kuhl E. Mechanics of the brain: perspectives, challenges, and opportunities. Biomech Model Mechanobiol. 2015 Oct; 14(5):931–965. https://doi.org/10.1007/s10237-015-0662-4 PMID: 25716305
30. Linninger AA, Xenos M, Sweetman B, Ponkshe S, Guo X, Penn R. A mathematical model of blood, cerebrospinal fluid and brain dynamics. J Math Biol. 2009 Dec; 59(6):729–759. https://doi.org/10.1007/s00285-009-0250-2 PMID: 19219605
31. Kurtcuoglu V. Computational fluid dynamics for the assessment of cerebrospinal fluid flow and its coupling with cerebral blood flow. Biomechanics of the Brain. Ed: Miller K. Springer, New York; 2011:169–188.
32. Buishas J, Gould IG, Linninger AA. A computational model of cerebrospinal fluid production and reabsorption driven by Starling forces. Croatian Medical Journal. 2014 Oct 15; 55(5):481–497. https://doi.org/10.3325/cmj.2014.55.481 PMID: 25358881

33. Linninger AA, Tangen K, Hsu CY, Frim D. Cerebrospinal fluid mechanics and its coupling to cerebrovascular dynamics. Annu Rev Fluid Mech. 2016 Jan 3; 48:219–257. https://doi.org/10.1146/annurev-fluid-122414-034321

34. Luce JM, Huseby JS, Kirk W, Butler J. A Starling resistor regulates cerebral venous outflow in dogs. J Appl Physiol Respir Environ Exerc Physiol. 1982 Dec; 53(6):1496–1503. https://doi.org/10.1152/jappl.1982.53.6.1496 PMID: 6759493

35. Cirovic S, Walsh C, Fraser WD, Gulino A. A Starling resistor regulates cerebral venous outflow in dogs. Aviat Space Environ Med. 2003 Feb; 74(2):125–131.

36. Gisolf J, van Lieshout JJ, van Heusden K, Pott F, Stok WJ, Karemaker JM. Human cerebral venous outflow pathway depends on posture and central venous pressure. J Physiol. 2004 Oct 1; 560(Pt 1):317–327. https://doi.org/10.1113/jphysiol.2004.070409 PMID: 15284348

37. De Simone R, Ranieri A, Sansone M, Marano E, Russo CV, Saccà F, Bonavita V. Dural sinus collapsibility, idiopathic intracranial hypertension, and the pathogenesis of chronic migraine. J Neurol Sci. 2019 May; 40(Suppl 1):59–70. https://doi.org/10.1007/s10072-019-03775-w

38. Louveau A, Plog BA, Antila S, Alitalo K, Nedergaard M, Kipnis J. Understanding the functions and relationships of the glymphatic system and meningeal lymphatics. J Clin Invest. 2017 Sep 1; 127(9):3210–3219. https://doi.org/10.1172/JCI90603 PMID: 28862640

39. Plog BA, Nedergaard M. The glymphatic system in central nervous system health and disease: past, present, and future. Annu Rev Pathol. 2018 Jan 24; 13:379–394. https://doi.org/10.1146/annurev-pathol-051217-111018 PMID: 29195051

40. Morgan WH, Yu DY, Alder VA, Cringle SJ, Cooper RL, House PH, Constable IJ. The correlation between cerebrospinal fluid pressure and retrolaminar tissue pressure. Invest Ophthalmol Vis Sci. 1998 Jul; 39(8):1419–1428. PMID: 9660490

41. Guidoboni G, Harris A, Carichino L, Arieli Y, Siesky BA. Effect of intraocular pressure on the hemodynamics of the central retinal artery: a mathematical model. Math Biosci Eng. 2014 Jun; 11(3):523–546. https://doi.org/10.3934/mbe.2014.11.523 PMID: 24506550

42. Carichino L, Guidoboni G, Siesky B, Amireskandari A, Januleviciene I, Harris A. Effect of intraocular pressure and cerebrospinal fluid pressure on the blood flow in the central retinal vessels. Integrated Multidisciplinary Approaches in the Study and Care of the Human Eye. Eds: Causin P, Guidoboni G, Sacco R, Harris A. Kugler Publications, Amsterdam. 2014;59–66.

43. Pedley TJ. The fluid mechanics of large blood vessels. Cambridge University Press; 1980.

44. Carlson BE, Arciero JC, Secomb TW. Theoretical model of blood flow autoregulation: roles of myogenic, shear-dependent, and metabolic responses. Am J Physiol Heart Circ Physiol. 2008 Oct; 295(4):H1572–1579. https://doi.org/10.1152/ajpheart.00262.2008 PMID: 18723769

45. Arciero JC, Carlson BE, Secomb TW. Theoretical model of metabolic blood flow regulation: roles of ATP release by red blood cells and conducted responses. Am J Physiol Heart Circ Physiol. 2008 Oct; 295(4):H1562–15671. https://doi.org/10.1152/ajpheart.00261.2008 PMID: 18689501

46. Arciero J, Harris A, Siesky B, Amireskandari A, Gershuny V, Pickrell A, Guidoboni G. Theoretical analysis of vascular regulatory mechanisms contributing to retinal blood flow autoregulation. Invest Ophthalmol Vis Sci. 2013 Aug 19; 54(8):5584–5593. https://doi.org/10.1167/iovs.12-11543 PMID: 23847315

47. Prada D, Harris A, Guidoboni G, Siesky B, Huang AM, Arciero J. Autoregulation and neurovascular coupling in the optic nerve head. Surv Ophthalmol. 2016 Mar-Apr; 61(2):164–186. https://doi.org/10.1016/j.survophthal.2015.10.004 PMID: 26498862

48. Bill A, Sperber GO. Control of retinal and choroidal blood flow. Eye (Lond). 1990; 4 (Pt 2):319–325. https://doi.org/10.1038/eye.1990.43

49. Kiel JW, Shepherd AP. Autoregulation of choroidal blood flow in the rabbit. Invest Ophthalmol Vis Sci. 1992 Jul; 33(8):2399–2410. PMID: 1634337

50. Reiner A, Fitzgerald MEC, Del Mar N, Li C. Neural control of choroidal blood flow. Prog Retin Eye Res. 2018 May;64:96–130. https://doi.org/10.1016/j.preteyeres.2017.12.001 PMID: 29229444

51. Mader TH, Gibson CR, Otto CA, Sargsyan AE, Miller NR, Subramanian PS, Hart SF, Lipsky W, Patel NB, Lee AG. Persistent asymmetric optic disc swelling after long-duration space flight: implications for pathogenesis. J Neuroophthalmol. 2017 Jun; 37(2):133–139. https://doi.org/10.1097/WNO.0000000000000467 PMID: 27930421

52. Lyubimov GA, Moiseeva IN, Stein AA. Dynamics of the intraocular fluid: Mathematical model and its main consequences. Fluid Dynam. 2007 Oct 1; 42(5):684–694. https://doi.org/10.1134/S001546280705002X

53. Brubaker RF. The effect of intraocular pressure on conventional outflow resistance in the enucleated human eye. Invest Ophthalmol. 1975 Apr; 14(4):286–292. PMID: 1123284

54. Murthy G, Marchbanks RJ, Watenpaugh DE, Meyer JU, Eliashberg N, Hargens AR. Increased intracranial pressure in humans during simulated microgravity. Physiologist. 1992 Feb; 35(1 Suppl):S184–185. PMID: 1589495

55. Lawley JS, Petersen LG, Howden EJ, Sarma S, Cornwell WK, Zhang R, Whitworth LA, Williams MA, Levine BD. Effect of gravity and microgravity on intracranial pressure. J Physiol. 2017 Mar 15; 595 (6):2115–2127. https://doi.org/10.1113/JP273557 PMID: 28092926

56. Fritzson P, Aronsson P, Lundvall H, Nyström K, Pop A, Saldamli L, Broman D. The OpenModelica modeling, simulation, and development environment. 46th Conference on Simulation and Modelling of the Scandinavian Simulation Society (SIMS2005), Trondheim, Norway, October 13-14; 2005.

57. Ravalico G, Toffoli G, Pastori G, Crocè M, Calderini S. Age-related ocular blood flow changes. Invest Ophthalmol Vis Sci. 1996 Dec; 37(13):2645–2650. PMID: 8977478

58. Grunwald JE, Hariprasad SM, DuPont J. Effect of aging on foveolar choroidal circulation. Arch Ophthalmol. 1998 Feb; 116(2):150–154. https://doi.org/10.1001/archopht.116.2.150 PMID: 9488265

59. Tarumi T, Zhang R. Cerebral blood flow in normal aging adults: cardiovascular determinants, clinical implications, and aerobic fitness. J Neurochem. 2018 Mar; 144(5):595–608. https://doi.org/10.1111/jnc.14234 PMID: 28986925

60. Schmidl D, Schmetterer L, Garhöfer G, Popa-Cherecheanu A. Gender differences in ocular blood flow. Curr Eye Res. 2015 Feb; 40(2):201–212. https://doi.org/10.3109/02713683.2014.906625 PMID: 24892919

61. Pointer JS. The diurnal variation of intraocular pressure in non-glaucomatous subjects: relevance in a clinical context. Ophthalmic Physiol Opt. 1997 Nov; 17(6):456–465. https://doi.org/10.1111/j.1475-1313.1997.tb00083.x PMID: 9666918

62. Rodriguez G, Warkentin S, Risberg J, Rosadini G. Sex differences in regional cerebral blood flow. J Cereb Blood Flow Metab. 1988 Dec; 8(6):783–789. https://doi.org/10.1038/jcbfm.1988.133 PMID: 3192645

63. Eklund A, Jóhannesson G, Johansson E, Holmlund P, Qvarlander S, Ambarki K, Wåhlin A, Koskinen LO, Malm J. The pressure difference between eye and brain changes with posture. Ann Neurol. 2016 Aug; 80(2):269–276. https://doi.org/10.1002/ana.24713 PMID: 27352140

64. Evans DW, Harris A, Garrett M, Chung HS, Kagemann L. Glaucoma patients demonstrate faulty autoregulation of ocular blood flow during posture change. Br J Ophthalmol. 1999 Jul; 83(7):809–813. https://doi.org/10.1136/bjo.83.7.809 PMID: 10381668

65. Longo A, Geiser MH, Riva CE. Posture changes and subfoveal choroidal blood flow. Invest Ophthalmol Vis Sci. 2004 Feb; 45(2):546–551. https://doi.org/10.1167/iovs.03-0757 PMID: 14744897

66. Alperin N, Hushek S, Lee S, Sivaramakrishnan A, Lichtor T. MRI study of cerebral blood flow and CSF flow dynamics in an upright posture: the effect of posture on the intracranial compliance and pressure. Intracranial Pressure and Brain Monitoring XII. Springer; 2005:177–181.

67. Werne A, Harris A, Moore D, BenZion I, Siesky B. The circadian variations in systemic blood pressure, ocular perfusion pressure, and ocular blood flow: risk factors for glaucoma?. Surv Ophthalmol. 2008 Nov-Dec; 53(6):559–567. https://doi.org/10.1016/j.survophthal.2008.08.021 PMID: 19026319

68. Conroy DA, Spielman AJ, Scott RQ. Daily rhythm of cerebral blood flow velocity. J Circadian Rhythms. 2005 Mar 10; 3(1):3. https://doi.org/10.1186/1740-3391-3-3 PMID: 15760472

69. Bhan A, Browning AC, Shah S, Hamilton R, Dave D, Dua HS. Effect of corneal thickness on intraocular pressure measurements with the pneumotonometer, Goldmann applanation tonometer, and Tono-Pen. Invest Ophthalmol Vis Sci. 2002 May; 43(5):1389–1392. PMID: 11980851

70. Siaudvytyte L, Januleviciene I, Ragauskas A, Bartusis L, Siesky B, Harris A. Update in intracranial pressure evaluation methods and translaminar pressure gradient role in glaucoma. Acta Ophthalmol. 2015 Feb; 93(1):9–15. https://doi.org/10.1111/aos.12502 PMID: 25043873

71. Dorner GT, Polska E, Garhöfer G, Zawinka C, Frank B, Schmetterer L. Calculation of the diameter of the central retinal artery from noninvasive measurements in humans. Curr Eye Res. 2002 Dec; 25 (6):341–345. https://doi.org/10.1076/ceyr.25.6.341.14231 PMID: 12789540

72. Dumskyj MJ, Eriksen JE, Doré CJ, Kohner EM. Autoregulation in the human retinal circulation: assessment using isometric exercise, laser Doppler velocimetry, and computer-assisted image analysis. Microvasc Res. 1996 May; 51(3):378–392. https://doi.org/10.1006/mvre.1996.0034 PMID: 8992235

73. Feke GT, Pasquale LR. Retinal blood flow response to posture change in glaucoma patients compared with healthy subjects. Ophthalmology. 2008 Feb; 115(2):246–252. https://doi.org/10.1016/j.ophtha.2007.04.055 PMID: 17689612

74. Feke GT, Hazin R, Grosskreutz CL, Pasquale LR. Effect of brimonidine on retinal blood flow autoregulation in primary open-angle glaucoma. J Ocul Pharmacol Ther. 2011 Aug; 27(4):347–352. https://doi.org/10.1089/jop.2011.0014 PMID: 21631365

75. Grunwald JE, DuPont J, Riva CE. Retinal haemodynamics in patients with early diabetes mellitus. Br J Ophthalmol. 1996 Apr; 80(4):327–331. https://doi.org/10.1136/bjo.80.4.327 PMID: 8703884

76. Kiel JW. Physiology of the intraocular pressure. Glaucoma. Ed: Fehér J. Academoiai Kiado, Budapest. 1998;79–107.

77. Linner E. A method for determining the rate of plasma flow through the secretory part of the ciliary body. Acta Physiol Scand. 1951 Apr 25; 22(2-3):83–86. https://doi.org/10.1111/j.1748-1716.1951.tb00755.x PMID: 14933129

78. Linner E. Ascorbic acid as a test substance for measuring relative changes in the rate of plasma flow through the ciliary processes. I. The effect of unilateral ligation of the common carotid artery in rabbits on the ascorbic acid content of the aqueous humour at varying plasma levels. Acta Physiol Scand. 1952 Jul 17; 26(1):57–69. https://doi.org/10.1111/j.1748-1716.1952.tb00891.x PMID: 12985397

79. Emeterio Nateras OS, Harrison JM, Muir ER, Zhang Y, Peng Q, Chalfin S, Gutierrez JE, Johnson DA, Kiel JW, Duong TQ. Choroidal blood flow decreases with age: an MRI study. Curr Eye Res. 2014 Oct; 39(10):1059–1067. https://doi.org/10.3109/02713683.2014.892997 PMID: 24655028

80. Strauss AL, Kedra AW. Experiences with a new procedure for the measurement of the ophthalmic artery pressure: ophthalmomanometry-Doppler. Med Instrum. 1987 Oct; 21(5):255–261. PMID: 2960872

81. Sit AJ, McLaren JW. Measurement of episcleral venous pressure. Exp Eye Res. 2011 Sep; 93(3):291–298. https://doi.org/10.1016/j.exer.2011.05.003 PMID: 21621536

82. Friedland AB. A mathematical model of transmural transport of oxygen to the retina. Bull Math Biol. 1978; 40(6):823–837. https://doi.org/10.1016/S0092-8240(78)80011-1

83. Apelblat A, Katzir-Katchalsky A, Silberberg A. A mathematical analysis of capillary-tissue fluid exchange. Biorheology. 1974 Jan; 11(1):1–49. https://doi.org/10.3233/BIR-1974-11101 PMID: 4824527

84. Wiederhielm C. Analysis of small vessel function. Physical Bases of Circulatory Transport: Regulation and Exchange. Eds: Reeve EB, Guyton AC. Saunders, Philadelphia. 1967;313–326.

85. Wiederhielm CA. Dynamics of capillary fluid exchange: a nonlinear computer simulation. Microvasc Res. 1979 Jul; 18(1):48–82. https://doi.org/10.1016/0026-2862(79)90017-7 PMID: 481245

86. Takahashi T, Nagaoka T, Yanagida H, Saitoh T, Kamiya A, Hein T, Kuo L, Yoshida A. A mathematical model for the distribution of hemodynamic parameters in the human retinal microvascular network. J Biorheol. 2009 Dec 1; 23(2):77–86. https://doi.org/10.1007/s12573-009-0012-1

87. Dielemans I, Vingerling JR, Algra D, Hofman A, Grobbee DE, de Jong PT. Primary open-angle glaucoma, intraocular pressure, and systemic blood pressure in the general elderly population. The Rotterdam Study. Ophthalmology. 1995 Jan; 102(1):54–60. https://doi.org/10.1016/S0161-6420(95)31054-8 PMID: 7831042

88. Mitchell P, Lee AJ, Wang JJ, Rochtchina E. Intraocular pressure over the clinical range of blood pressure: Blue Mountains eye study findings. Am J Ophthalmol. 2005 Jul; 140(1):131–132. https://doi.org/10.1016/j.ajo.2004.12.088 PMID: 16038656

89. Xu L, Wang H, Wang Y, Jonas JB. Intraocular pressure correlated with arterial blood pressure: the Beijing eye study. Am J Ophthalmol. 2007 Sep; 144(3):461–462. https://doi.org/10.1016/j.ajo.2007.05.013 PMID: 17765433

90. Ren R, Jonas JB, Tian G, Zhen Y, Ma K, Li S, Wang H, Li B, Zhang X, Wang N. Cerebrospinal fluid pressure in glaucoma: a prospective study. Ophthalmology. 2010 Feb; 117(2):259–266. https://doi.org/10.1016/j.ophtha.2009.06.058 PMID: 19969367

91. Bill A. The uveal venous pressure. Arch Ophthalmol. 1963 Jun; 69:780–782. https://doi.org/10.1001/archopht.1963.00960040786021 PMID: 13968253

92. Taibbi G, Cromwell RL, Zanello SB, Yarbough PO, Ploutz-Snyder RJ, Godley BF, Vizzeri G. Ocular outcomes evaluation in a 14-day head-down bed rest study. Aviat Space Environ Med. 2014 Oct; 85(10):983–992. https://doi.org/10.3357/ASEM.4055.2014 PMID: 25245897